Am J Physiol Renal Physiol 323: F120–F140, 2022.
First published June 6, 2022; doi:10.1152/ajprenal.00072.2022

american physiological society

AMERICAN JOURNAL OF PHYSIOLOGY
RENAL PHYSIOLOGY

RESEARCH ARTICLE

Molecular Basis of Kidney Injury and Repair

Maladaptation of renal hemodynamics contributes to kidney dysfunction resulting from thoracic spinal cord injury in mice

Patrick Osei-Owusu,[1] Eileen Collyer,[2] Shelby A. Dahlen,[1] Raisa E. Adams,[1] and Veronica J. Tom[2]

[1]*Department of Physiology and Biophysics, Case Western Reserve University School of Medicine, Cleveland, Ohio and*
[2]*Department of Neurobiology and Anatomy, Drexel University College of Medicine, Philadelphia, Pennsylvania*

Abstract

Renal dysfunction is a hallmark of spinal cord injury (SCI). Several SCI sequalae are implicated; however, the exact pathogenic mechanism of renal dysfunction is unclear. Herein, we found that T3 (T3Tx) or T10 (T10Tx) complete thoracic spinal cord transection induced hypotension, bradycardia, and hypothermia immediately after injury. T3Tx-induced hypotension but not bradycardia or hypothermia slowly recovered to levels in T10Tx SCI and uninjured mice ~16 h after injury as determined by continuous radiotelemetry monitoring. Both types of thoracic SCI led to a marked decrease in albuminuria and proteinuria in all phases of SCI, whereas the kidney injury marker neutrophil gelatinase-associated lipocalin rapidly increased in the acute phase, remaining elevated in the chronic phase of T3Tx SCI. Renal interstitial and vascular elastin fragmentation after SCI were worsened during chronic T3Tx SCI. In the chronic phase, renal vascular resistance response to a step increase in renal perfusion pressure or a bolus injection of angiotensin II or norepinephrine was almost completely abolished after T3Tx SCI. Bulk RNA-sequencing analysis showed enrichment of genes involved in extracellular matrix remodeling and chemokine signaling in the kidney from T3Tx SCI mice. The serum level of interleukin-6 was elevated in the acute but not chronic phase of T3Tx and T10Tx SCI, whereas the serum amyloid A1 level was elevated in both acute and chronic phases. We conclude that tissue fibrosis and hemodynamic impairment are involved in renal dysfunction resulting from thoracic SCI; these pathological alterations, exacerbated by high thoracic-level injury, is mediated at least partly by renal microvascular extracellular matrix remodeling.

NEW & NOTEWORTHY Urinary complications resulting from thoracic spinal cord injury (SCI) greatly affects quality of life and contributes to morbidity and mortality in patients with SCI. Herein, we showed that thoracic SCI initiates changes in the structure and function of the renal microvasculature that leads to autoregulation failure in the chronic phase of high thoracic-level injury. Our study identified extracellular matrix regulators and cytokine/chemokine signaling as potential targets for developing novel therapeutics for restoring renal function following SCI.

extracellular matrix; fibrosis; renal autoregulation; thoracic spinal cord injury; vascular remodeling

INTRODUCTION

Spinal cord injury (SCI) often results in autonomic dysfunction that contributes to mortality and morbidity (1, 2). This includes altered renal function that contributes to urinary complications including excessive urine production at nighttime or nocturnal polyuria, characterized by amplified diuresis observed during bed rest and sleep (3, 4). SCI also disrupts the diurnal variation of circulating antidiuretic hormone (ADH), resulting in a persistently low level of this endogenous vasopressin receptor ligand that stimulates water reuptake by the distal nephron (5, 6). There is accumulating evidence that the reduced ability of the kidney to concentrate urine due to impaired vasopressin-mediated water reuptake plays a causal role in excessive urine production during chronic SCI (5–8). Accordingly, most studies of the causes and treatment of SCI-related urine overproduction have focused on vasopressin-mediated water reuptake by the distal nephron (3, 9–11). However, in addition to tubular reabsorption of water and electrolytes, urine production rate and volume are also dependent on renal hemodynamics controlling renal plasma flow and glomerular filtration rate (GFR), both driven by systemic and renal perfusion pressure (RPP). In both individuals with SCI and experimental rodent SCI models, the acute phase of high-level SCI is characterized by a marked decline in renal plasma flow and GFR, accompanied by decreased urine output (12). This decline in renal function is thought to be mediated by the precipitous fall in RPP due to acute hypotension following the injury (13). In the chronic phase of high-level SCI, urine output

Correspondence: P. Osei-Owusu (pxo70@case.edu); V. J. Tom (vjt25@drexel.edu).
Submitted 18 March 2022 / Revised 31 May 2022 / Accepted 31 May 2022

markedly increases, particularly during bed rest and sleep (3), as resting blood pressure recovers close to the preinjury level and becomes more stable, except during instances of autonomic dysreflexia (AD) that elicit huge swings in systemic pressure. How changes in systemic pressure during the initial phase of SCI and subsequent AD in the chronic phase affect renal hemodynamics and contribute to renal dysfunction are poorly explored.

The kidney, sometimes described as the "master regulator" of long-term blood pressure, is the primary regulator of water and electrolyte balance, controlling extracellular fluid volume and thus cardiac output (14–17). This function of the kidney depends on plasma filtration in the glomerulus and reabsorption of water and ions, mainly Na^+, along the nephron. Plasma filtration at the glomerulus is driven by a positive net balance between the Starling forces, oncotic and hydrostatic pressures, within the lumen of the endothelial network of the glomerular tuft and those in the Bowman's space. In the absence of any tubular obstruction, the net positive pressure in the glomerular capillary lumen determines GFR and the volume of the ultrafiltrate getting into Bowman's space and traveling along the nephron. This net driving pressure is determined in part by renal plasma flow that is subject to the overall renal vascular resistance (RVR), which is, in turn, determined by the level of tone of both pre- and postglomerular arterioles (18–21). To maintain a net positive driving pressure for GFR, the tone of the resistance vasculature in the kidney changes in response to a change in RPP, an autoregulation phenomenon whereby an increase or a decrease in RPP triggers vasoconstriction to increase RVR or vasodilatation to decrease resistance, respectively (22). Renal autoregulation comprises two mechanisms: myogenic response and tubuloglomerular feedback (TGF). Myogenic response is a smooth muscle intrinsic property that mediates a rapid arteriolar constriction in response to a mechanical stretch elicited by increases in intraluminal pressure (23–25). The slower autoregulatory mechanism, TGF, is triggered by sensing of Na^+ by the macula densa in the distal convoluted tubule of the juxtaglomerular apparatus, thereby causing the release of vasoactive ligands and/or activation of mechanosensitive ion channels inducing reactivity of the afferent arteriole (23, 26–29). Renal autoregulation operates within a certain blood pressure range (23, 30). Systemic pressure above or below these limits of autoregulation, as occurs during various phases of SCI, can cause renal plasma flow to fluctuate in the same direction as RPP.

In the present study, we compared renal hemodynamics and autoregulation after acute or chronic complete thoracic level 3 (T3) or thoracic level 10 (T10) spinal cord transection in the mouse and determined how high- or low-thoracic SCI alters the structure and function of the kidney. In addition, we performed transcriptomic analysis to gain a deeper understanding of the molecular mechanisms mediating the effects of SCI on the kidney.

MATERIALS AND METHODS

Animals

We used adult (2- to 6-mo-old) female C57 black 6 mice purchased from Jackson Laboratories for all experiments. All animal procedures and the protocol for the study were approved by the Institutional Animal Care and Use Committee of Drexel University, in accordance with the United States animal welfare act. On arrival, animals were allowed to acclimate for at least 1 wk at 22°C and a 12:12-h light-dark cycle with access to food and water ad libitum in our institution's animal facility. Animals were randomly assigned to one of the following three groups: complete spinal transection at T3 (T3Tx), complete spinal transection at T10 (T10Tx), and uninjured (intact spinal cord). Following the surgical procedures, animals received ampicillin (200 mg/kg), meloxicam (PennVet, 2 mg/kg), and lactated Ringer's solution perioperatively and were placed in their cages in a thermal barrier to recover, as previously described (31–33). We performed manual bladder expressions at least twice a day on all SCI animals for the duration of the study.

Thoracic Spinal Transection Surgery

Under isoflurane anesthesia, the spinal cord at T3 or T10 was exteriorized by laminectomy of the T2 or T9 vertebral processes, respectively, as previously described (31, 32). A small incision was made with a microknife in the dura overlaying the vertebral column at T3 or T10, followed by running a 30-gauge needle in the incision to ensure complete transection. Following the transection verification, the cavity was filled with gel foam saturated with normal saline to stop bleeding. The gel foam was left in place, and the muscle overlaying the dura was sutured closed with a 4-0 vicryl suture followed by stapling the skin.

Conscious Hemodynamics and Temperature Monitoring by Radiotelemetry

Blood pressure, heart rate (HR), and body temperature were monitored in conscious mice using radiotelemetry, as we have previously described (34). Radiotelemetry implantation surgery was performed under isoflurane anesthesia at least 1 wk before spinal transection to allow enough time for recovery and to acquire preinjury parameters, as we have previously reported (35). Radiotelemetry catheters (model HD-X10, Data Sciences, St. Paul, MN) were placed in the ascending aorta by way of the right common carotid artery, as we have previously described (36). The transmitter was placed subcutaneously on the lower back of the animals for transmission of blood pressure and body temperature data. Using the Ponemah Data Acquisition System from Data Sciences, we recorded baseline diurnal blood pressure and HR as well as body temperature of conscious mice 24 h before thoracic spinal transection surgery. One hour after T3Tx or T10Tx, when the mice were awake and fully alert and with a heating pad placed between the bottom of the cage and the telemetry receivers, continuous telemetry recording was resumed at a sampling rate of 1,000 cycles/s for 24 h. The recording session was repeated once a week for a total of 4 wk. The acquired data were resampled at reduced averages of continuous temperature, systolic blood pressure (SBP), diastolic blood pressure (DBP), mean arterial pressure (MAP), and HR recordings in 1-h intervals over 24 h.

Assessment of Naturally Occurring AD

Mice were individually placed in cages and positioned on telemetry receivers (RC-1, Data Sciences). Baseline recordings of all animals after telemeter implantation but before SCI were obtained to ensure that HR and MAP values were within a normal range, confirming that the catheters were not occluded. At every other week from 2 to 8 wk after SCI, MAP and HR were monitored continuously for 24 h, while animals moved freely in their cages (MAP and HR values sampled every 2 s, Dataquest A.R.T. and Ponemah acquisition software, Data Sciences). Similar to what we have previously described (31, 37), to identify naturally occurring AD events, these data from individual animals at each time point were analyzed in MATLAB. Rolling MAP and HR baselines were established by continuously averaging a 6-m period. AD events were defined as when MAP was at least 10 mmHg greater than baseline for at least 30 s and was accompanied by bradycardia of at least 10 beats/min. All "detected" events were visually verified by a blinded observer according to the predefined changes in MAP and HR. All false positive events were disregarded. Any events that occurred within 2 min of each other were considered to be one event. Any detected events within 15 min of manual bladder expression were not included in additional comparative analyses. Once an event was verified, the average MAP during the event, the change in MAP from baseline, the HR during the event, and the duration of the bout was calculated.

Measurement of Plasma Serum Amyloid A1 and Interleukin-6 Levels

Blood samples collected at the end of renal hemodynamic assessment were centrifuged at 3,000 rpm for 5 min at room temperature to obtain plasma. Levels of serum amyloid A1 (SAA1) and interleukin (IL)-6 were measured using ELISA kits by following the manufacturer's instructions (SAA1 kit: Thermo Fisher and IL-6 kit: Ethos Biosciences, Newtown Square, PA).

Determination of Urine Neutrophil Gelatinase-Associated Lipocalin, Creatinine, Albumin, and Protein Levels

For the determination of urine levels of neutrophil gelatinase-associated lipocalin (NGAL) and albumin, we used urine samples collected during the morning session of bladder expression in SCI animals at 24 h after injury or at the same time of day 4 wk later. In intact animals, spot urine was collected at the same time of day as in SCI mice. We used commercially available kits for NGAL and creatinine from R&D Biosystems (Minneapolis, MN) and microalbumin from Ethos Biosciences (Ethos Biosciences) by following the manufacturer's assay protocols. Total urine protein determined by a Pierce BCA Protein Assay kit (Thermo Fisher Scientific, San Jose, CA) was used to normalize NGAL values. Because T3Tx mice tend to lose more muscle mass and hence have lower body weight over the 4-wk period, we normalized urine protein and microalbumin concentrations by the average kidney weight of the mouse. In cases where kidney weight was not recorded, we used the mean kidney weight of the group for the subject. For 24-h proteinuria and microalbuminuria, we normalized values using urine creatinine concentration.

Acute Elevation of RPP by Arterial Occlusion or by Vasoactive Agent Administration

Mice were surgically instrumented as we have previously described (34). Briefly, a fluid-filled mouse carotid artery catheter (MA-10, SAI, IL) and a PE-10 jugular vein catheter were implanted for blood pressure measurement and drug delivery, respectively. The left renal artery and abdominal aorta and its major suprarenal branches were visualized and freed from the surrounding fascia via the retroperitoneal cavity, following incision of the skin and dorsal abdominal muscle at the left flank. This was followed by loosely placing pieces of 5-0 silk around the celiac and superior mesenteric arteries. A perivascular flow probe (0.5PSB Nanoprobe with handle, Transonic) was placed around the left renal artery for renal blood flow (RBF) monitoring. After 15 min of equilibration, boluses of angiotensin II (ANG II; 0.1 or 1 μg/kg) and norepinephrine (NE; 1, 10, or 50 μg/kg) were administered via the jugular vein catheter in 10-μL volumes. Blood pressure and RBF were allowed to return to preinjection levels after each administration. Approximately 10 min after the last drug administration, the ligatures around the celiac and superior mesenteric arteries were tightened almost simultaneously to occlude the vessels while blood pressure and RBF were monitored continuously. At the end of 15 min of recording, the experiment was terminated, and the kidneys were harvested for weight determination and fixation or flash frozen. Hemodynamic data were recorded and analyzed with LabChart 8 (ADInstruments, Colorado Springs, CO).

Histological Analysis

Assessment of tissue fibrosis.

Kidneys harvested from terminal renal hemodynamics experiments were fixed in 10% formalin solution and embedded in paraffin. Tissue embedding, sectioning, and histological staining were performed in the Anatomical Pathology Core facility at Thomas Jefferson University (Philadelphia, PA) and at the Tissue Procurement Core at University Hospitals (Cleveland, OH). To determine the level of perivascular and interstitial fibrosis, the extent of perivascular and interstitial collagen deposition indicated by blue Masson's trichrome staining of stitched bright-field microscopic images of sections were analyzed by an individual blinded to the identity of the samples or experimental design. The level of fibrosis was expressed as the percent area of the kidney section with trichrome stain.

Quantification of collagen deposition.

Collagen deposition and elastin organization in the medial layer and in the internal and external elastic laminae of renal microvessels and glomeruli were visualized by Movat staining. All slides were imaged using a Keyence BZ-X700 microscope, and the acquired images were processed for collagen quantification using National Institutes of Health ImageJ software. Briefly, histological images of kidney blood vessels and glomeruli were uploaded into ImageJ, and the "Analyze > Set Scale" command was used to convert the image scale to micrometers. Next, the ImageJ

color_segmentation plugin was used to define colored pixels of stained regions of interest associated with collagen (yellow), elastin (dark purple), and red blood cells (red) within the perivascular space, vessel wall, and renal corpuscle in the histological sections. The *K*-means clustering method was used to generate a color-segmented copy of the original histological image. Next, the images were converted to grayscale using the "Image > Type > RGB Stack" command, splitting the image into red, green, and blue channels. The RGB stack that provided the best contrast of extracellular matrix (ECM) components was selected, and the "Image > Adjust > Threshold" function used to highlight stained components of interest in red. Next, the image selection tool was used to outline regions of interest (perivascular space, blood vessels excluding the vessel lumen, and renal corpuscles) containing stained collagen fibers. Finally, we used the "analyze > measure" function in ImageJ to calculate the area percentage of the collagen highlighted red (due to threshold adjustment of the grayscale image) within the outlined regions of interest in each slide.

Renal microvascular elastin fragmentation analysis.
The level of microvascular elastin organization, including in the internal elastic lamina (IEL), tunica media, and external elastic lamina (EEL) of Movat-stained histological sections of the kidney was scored on a scale of 0–4. The following scoring parameters were used to determine the degree of elastin fragmentation: 1 = minimal elastin fragmentation (15% or less), 2 = moderate elastin fragmentation (20–40%), 3 = serious elastin fragmentation (50–70%), and 4 = severe elastin fragmentation (75% or more). Vessels appearing distorted (poor resolution of the IEL, EEL, and tunica media) due to the tissue sectioning process were excluded from the scoring analysis. Approximately 12–20 vessels were scored per kidney section. Tissue scoring was blinded and performed by two observers. Mean scores were used for statistical analysis.

Glomerular congestion.
Roughly 30–35 glomeruli per slide were randomly selected from images of Movat-stained histological sections of the kidney, and the severity of glomerular congestion was scored according to the abundance of red blood cells observed within the renal corpuscle. The following scoring parameters were used to determine the degree of glomerular congestion: 1 = minor congestion, 2 = moderate congestion, 3 = serious congestion, and 4 = severe congestion. Scoring was performed by two blinded observers. Mean scores were taken for statistical analysis.

Bulk RNA Sequencing

Adult female mice (n = 4 per group) were subjected to T3Tx or T10Tx SCI under anesthesia. Four weeks later, the kidneys were harvested, weighed, and flash frozen after acute recording of blood pressure and RBF under anesthesia. Kidneys from intact mice without SCI were also harvested after the animals had been subjected to the same surgical procedures for blood pressure and RBF recordings. RNA was isolated from ~20 mg of frozen kidney samples using the RNeasy Mini Kit (Qiagen) by following the manufacturer's protocol, including sample treatment with DNase I to remove potential genomic DNA contamination. First-pass RNA quality was assessed using a NanoDrop 2000 Microvolume Spectrophotometer (Thermo Fisher Scientific). RNA quality control and library preparation were performed by the Case Western Reserve University Genomics Core facility (https://genomics.case.edu) using an Invitrogen Qubit Fluorometer RNA assay with an AATI Fragment Analyzer RNA assay to determine concentration and the integrity of RNA and an Illumina NextSeq High Output flowcell–1 × 75 bp run, respectively. FastQ files were submitted to the Case Western Reserve University Institute for Computational Biology for sequence alignment and transcriptomic analysis using ADVAITA next-generation bioinformatics software. The *iPathwayGuide* was used for Gene Ontology (GO) analysis for the identification of enriched terms and overrepresented genes in sets of genes with measured expression. Direct and separate comparisons of uninjured versus T3Tx and uninjured versus T10Tx samples were used to determine injury-specific GO terms with significant enrichment and level-specific effects on differential expression of genes and signaling pathways.

Gene Expression Analysis by Real-Time PCR

Total RNA was extracted from kidney samples using an RNA isolation kit and by following the manufacturer's (Qiagen) instruction. RNA was purified using the Purelink RNA Mini Kit (Thermo Fisher Scientific) and then reverse transcribed using a Maxima First Strand cDNA Synthesis Kit (Thermo Fisher Scientific), all according to the manufacturer's instructions. The following primer probes were used in the real-time PCR assays with TaqMan gene expression master mix (Thermo Fisher Scientific): matrix metalloproteinase 3 (*Mmp3*), Mm00440295 m1; collage type XIII-α_1 (*Col13a1*), Mm00483507_m1; *Saa1*, Mm00656927_g1; ADAM metallopeptidase with thrombospondin type 1 motif 1 (*Adamts1*), Mm01344169 m1; ADAM metallopeptidase with thrombospondin type 1 Motif 4 (*Adamts4*), Mm00556068_m1; chemokine (C-X-C motif) ligand 10 (*Cxcl10*), Mm00445235_m1; VEGFA (*Vegfa*), Mm00437306_m1; IL-6 (*Il6*), Mm00446190_m1; IL-11 (*Il11*), Mm00434162_m1; and GAPDH (*Gapdh*), Mm99999915_g1. The ΔC_t method (where C_t is threshold cycle) was used to calculate mRNA expression after normalization to *Gapdh* expression.

Statistics

All values are presented as means ± SE. We used two-way ANOVA for statistical analysis of all data, using repeated-measures ANOVA for hemodynamic data and randomized group analysis for all other comparisons. Where there was an effect of one or both factors and/or an interaction between the factors in the two-way ANOVA, we used Newman–Keuls post hoc analysis to determine within-group differences from baseline and between-group differences from intact, uninjured mice or Dunnett's test for comparison of T3Tx and T10Tx with uninjured control. All comparisons with a P value of <0.05 were considered statistically significant. All statistical analyses were performed using GraphPad Prism 8.1.1 software for Mac OS X (GraphPad Software, San Diego, CA).

RESULTS

High Thoracic-Level SCI Induces Hypotension Accompanied by Profound Bradycardia and Hypothermia

Prior to SCI, baseline blood pressure, HR, and body temperature were similar among all groups of mice. One day after T3Tx SCI, average daytime and nighttime SBP dropped by ~30 mmHg, accompanied by a marked decrease in HR (~250 beats/min) and body temperature (~36°C–30°C; Fig. 1, blue bars), consistent with previous reports (2, 38–40). One week after T3Tx and for the rest of the post-T3Tx monitoring period, body temperature and HR returned close to preinjury levels and remained stable, whereas SBP persistently trended lower than the baseline level. In contrast to the observations in T3Tx SCI mice, SBP, HR, and body temperature of T10Tx SCI mice returned to preinjury levels within 24 h of injury and remained at these levels for the duration of the monitoring period (Fig. 1, black bars).

High Thoracic-Level Injury Prolongs the Recovery of SCI-Induced Hypotension, Bradycardia, and Hypothermia

To assess the impact of injury level on the dynamics of circulatory function, we examined the diurnal rhythm of blood pressure, HR, and body temperature before injury and shortly after T3Tx or T10Tx SCI by radiotelemetry monitoring. Before injury, all mice had similar diurnal blood pressure, HR, and temperature rhythms, with high values recorded during the active period at nighttime and low

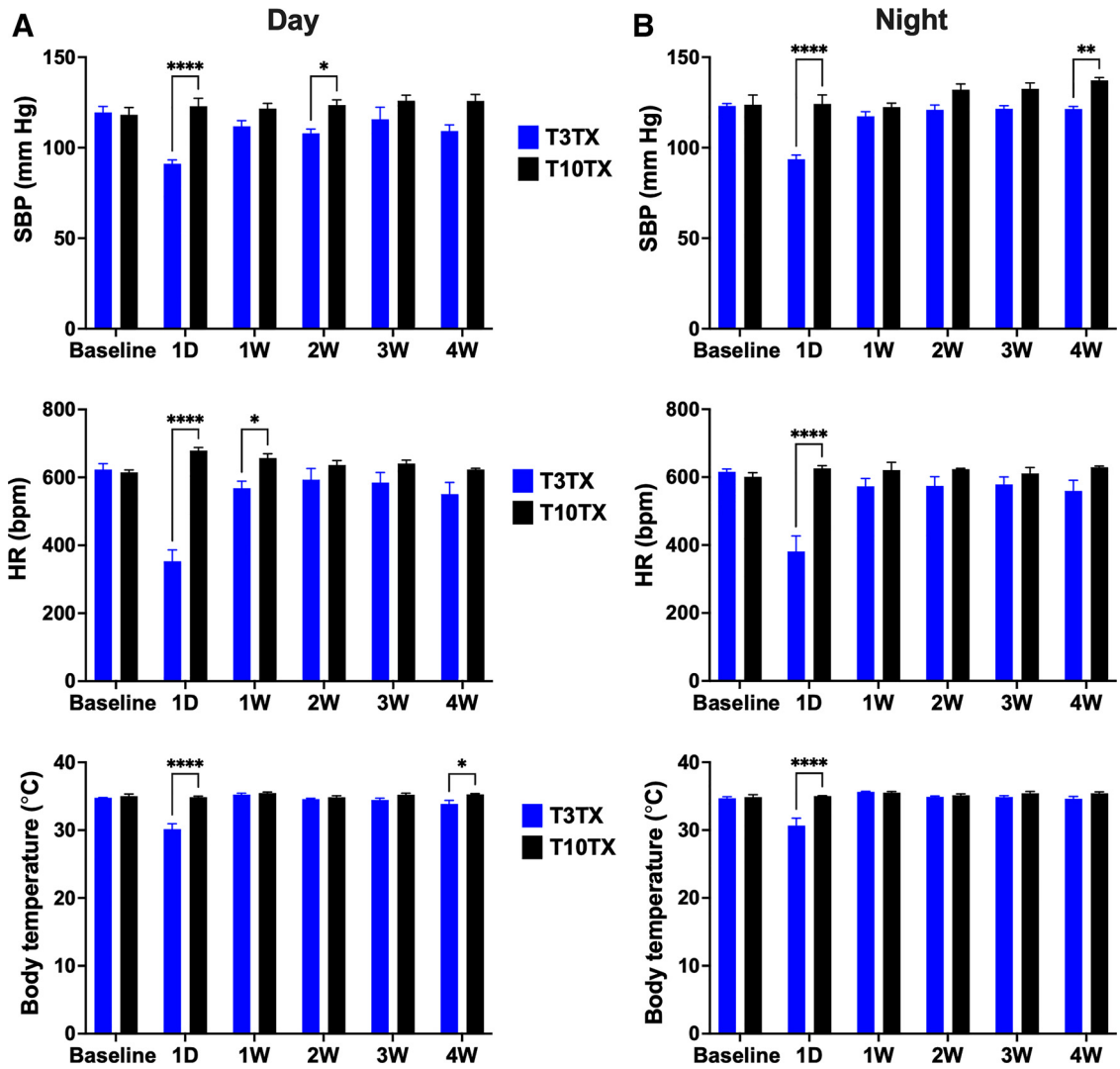

Figure 1. Spinal cord transection at thoracic level 3 (T3Tx) causes an acute decrease in diurnal systolic blood pressure (SBP), heart rate [HR; in beats/min (bpm)], and body temperature. Resting hemodynamics and body temperature were recorded before injury and after complete T3Tx ($n = 3$) or spinal cord transection at thoracic level 10 (T10Tx; $n = 5$) by radiotelemetry starting 1–24 h after injury and every week for 4 wk. *A* and *B*: compared with preinjury baseline, T3Tx caused a precipitous drop in daytime and nighttime SBP, HR, and body temperature within the first 24 h of injury, whereas T10Tx had no effect within the same time period. Once recovered in T3Tx spinal cord-injured mice, HR and body temperature remained stable and close to preinjury levels; however, SBP trended lower relative to levels in T10Tx spinal cord-injured mice, particularly at 2 and 4 wk after injury. Values are means ± SE. Statistical significance was determined by two-way repeated-measures ANOVA followed by Newman–Keuls post hoc tests for within- and between-group comparisons. *$P < 0.05$ and ****$P < 0.001$, T3Tx vs. T10Tx at 2 wk and 1 day postinjury, respectively.

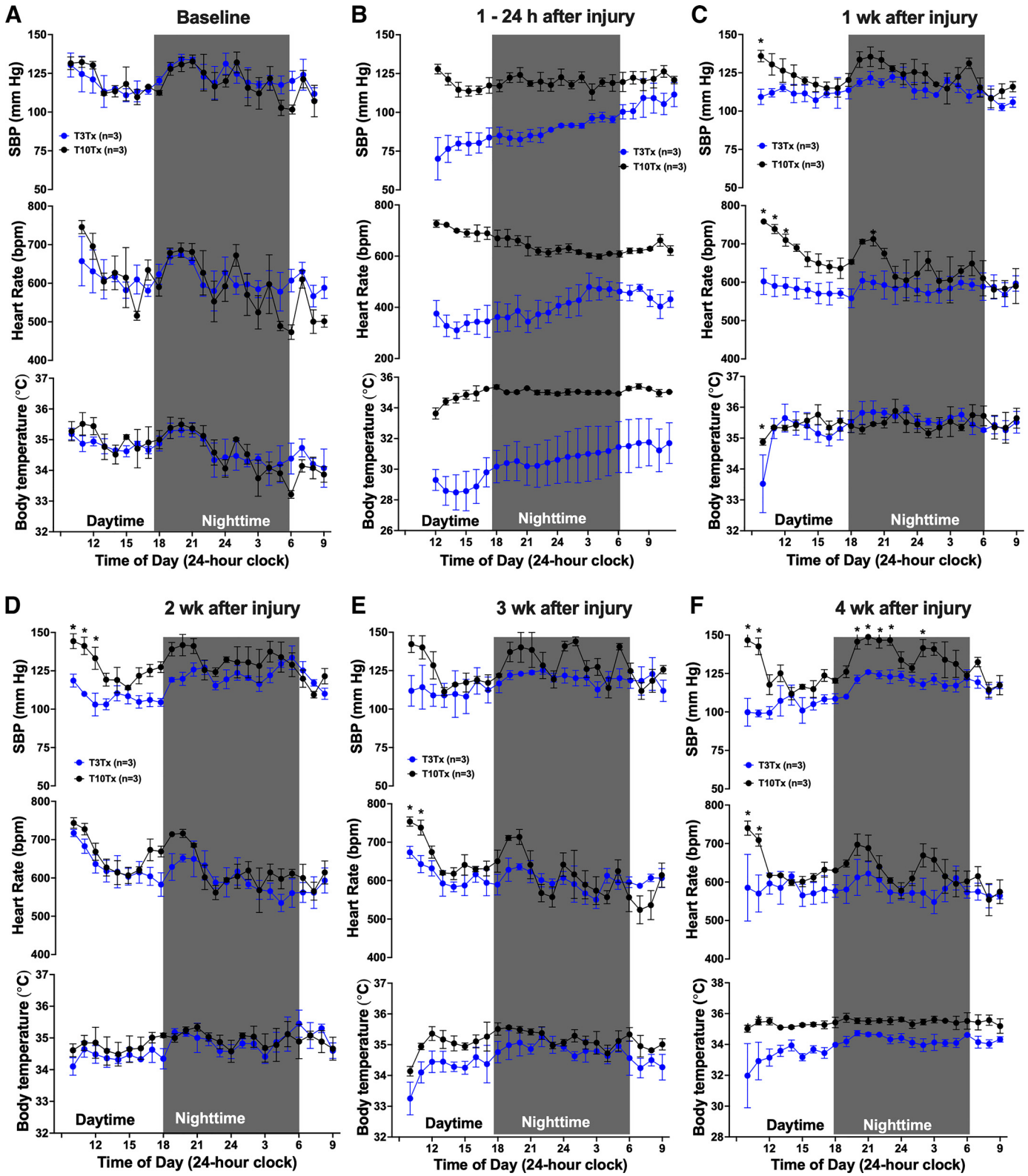

Figure 2. High and low thoracic-level injury disrupts diurnal blood pressure [systolic blood pressure (SBP)], heart rate [HR; in beats/min (bpm)], and body temperature rhythm. *A*: rhythms in diurnal SBP, HR, and body temperature of spinal cord transection at thoracic level 3 (T3Tx; $n = 3$) and thoracic level 10 (T10Tx; $n = 5$) spinal cord-injured mice were normal prior to injury. *B*: shortly after T3Tx injury, all three parameters fell sharply and slowly recovered, approaching preinjury levels after ~16 h. Although SBP, HR, and body temperature were maintained in T10Tx mice, the diurnal rhythm was abolished in T3Tx within 24 h of injury. *C*–*F*: diurnal rhythm was reestablished 1 wk after injury; however, SBP remained lower in T3Tx mice 4 wk later. Values are means ± SE. Statistical significance was determined by two-way repeated-measures ANOVA followed by Newman–Keuls post hoc tests for between-group comparisons. *$P < 0.05$, T3Tx vs. T10Tx.

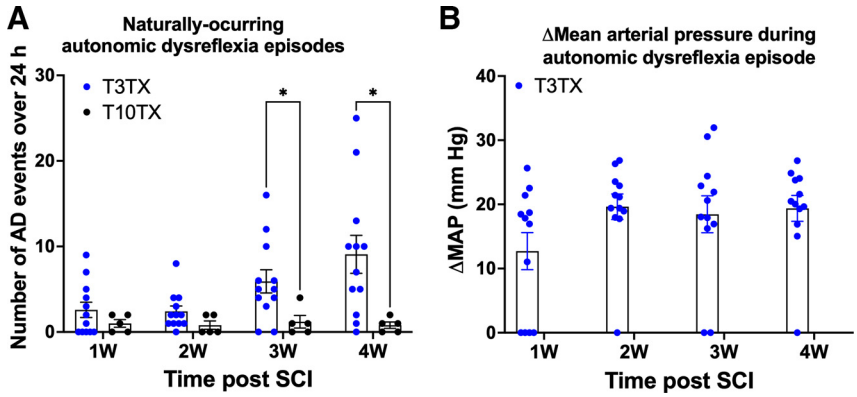

Figure 3. High thoracic-level injury leads to high episodes of autonomic dysreflexia (AD) in female mice. *A*: summary of spontaneously occurring AD episodes at 1, 2, 3, and 4 wk after spinal cord transection at thoracic level 3 (T3Tx) or thoracic level 10 (T10Tx). Episodes of AD were identified as spontaneous spikes in mean arterial pressure (MAP) detected using a custom-written MATLAB algorithm followed by manual inspection of the 24-h MAP telemetry tracing. *B*: summary of peak changes in MAP (ΔMAP) during AD episodes. MAP increased by an average of 15 mmHg during AD in T3Tx spinal cord-injured (SCI) mice. Values are means ± SE. Statistical significance was determined by mixed model two-way ANOVA followed by Newman–Keuls post hoc tests for between-group comparisons at given time points. $*P < 0.05$, T3Tx vs. T10Tx.

values in the daytime when animals mostly rest (Fig. 2*A*). In T3Tx mice, the injury abolished diurnal rhythm, as blood pressure began to rise slowly within the first 24 h following a marked decline precipitated by the high thoracic-level SCI, reaching the control level ~16 h after injury (Fig. 2*B*). HR and body temperature followed a similar trend of recovery as SBP; however, both parameters remained well below preinjury levels 16–24 h after the initial T3Tx. All three parameters in T3Tx mice remained slightly lower than pre-SCI levels at 1, 2, 3, and 4 wk after injury, with the difference becoming more noticeable at nighttime (Fig. 2, *C–F*). In T10Tx mice, blood pressure, HR, and body temperature remained at preinjury levels from 1 h after injury and throughout the 4-wk recording sessions. In both groups of SCI mice, the diurnal rhythm in blood pressure, HR, and body temperature were reestablished as early as 1 wk after injury (Fig. 2*C*).

AD Events Progressively Increase in High Thoracic-Level Injury

Autonomic dysreflexia develops in rodent models of severe high-thoracic level SCI, such as T3Tx, and episodes are commonly triggered by noxious sensory stimuli such as constipation and a full bladder. We and others have shown that AD gets progressively exaggerated by analyzing longitudinal blood pressure and HR monitoring by radiotelemetry (31, 37, 41–44). To determine the extent of AD in the animals in this study, we reanalyzed the 24-h blood pressure and HR radiotelemetry recordings acquired every week for 4 wk from the time of either T3Tx or T10Tx injury, part of which is shown in Fig. 2. As shown in Fig. 3, naturally occurring AD events (i.e., AD events not elicited experimentally) were detected as early as 1 wk after injury in both T3Tx and T10Tx SCI mice. Whereas the number of AD events detected in

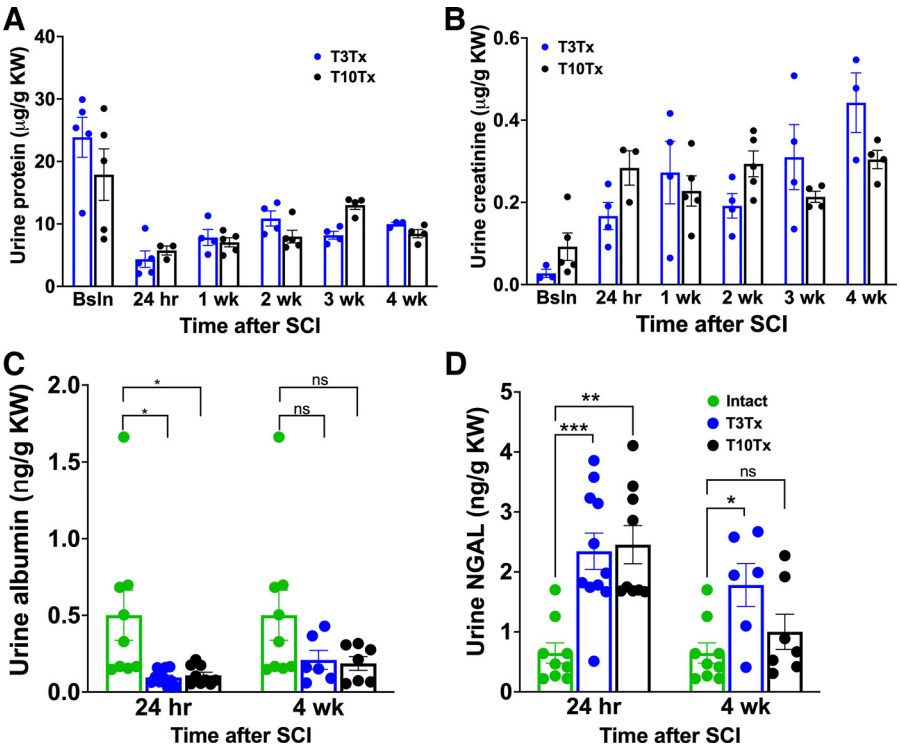

Figure 4. Thoracic-level injury leads to a chronic decline in proteinuria and microalbuminuria accompanied by elevated levels of the kidney injury marker neutrophil gelatinase-associated lipocalin (NGAL). *A*: time course of urine protein excretion before [baseline (Bsln)] and after spinal cord transection at thoracic level 3 (T3Tx) and thoracic level 10 (T10Tx). Both types of spinal cord injury (SCI) led to a marked decrease in proteinuria. *B*: time course of urine creatinine excretion showing a sharp increase in 24 h after either T3Tx or T10Tx relative to preinjury levels (Bsln). Although the increase in urine creatinine excretion plateaued after the initial rise at 24 h after T10Tx, it progressively rose in T3Tx mice, showing the highest excretion at 4 wk postinjury. *C*: summary of microalbuminuria in uninjured, T3Tx, and T10Tx SCI mice at 24 h and 4 wk postinjury. Like proteinuria, microalbuminuria was suppressed after both injury types in the acute and chronic phases of the injury. *D*: summary of the urine level of the kidney injury marker NGAL. Urine NGAL was markedly elevated in the acute phase of thoracic SCI and remained elevated in T3Tx mice 4 wk later, whereas it fell in T10Tx mice to a similar level in uninjured control. Values are means ± SE. Statistical significance was determined by mixed model two-way ANOVA followed by Dunnett's post hoc tests for comparisons with uninjured control at the indicated time points. $*P < 0.05$, $**P < 0.01$, and $***P < 0.001$ vs. uninjured control. KW, kidney weight.

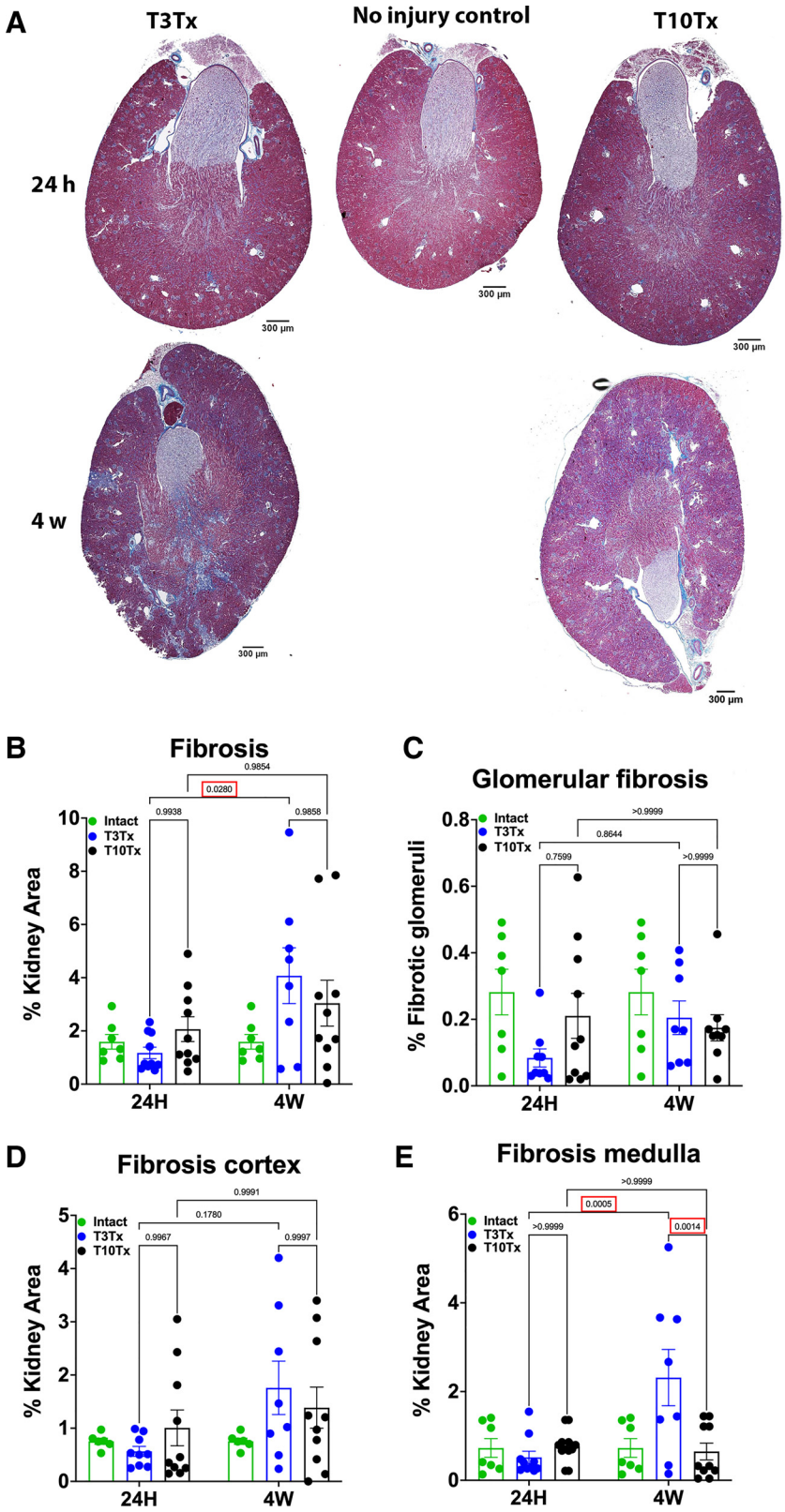

Figure 5. High thoracic-level injury exacerbates spinal cord injury (SCI)-induced renal fibrosis. *A*: representative photomicrographs of kidney sections (5 µm each) prepared from uninjured control, spinal cord transection at thoracic level 3 (T3Tx), and spinal cord transection at thoracic level 10 (T10Tx) injured mice at 24 h and 4 wk postinjury. *B*: summary of the overall fibrosis score of kidney sections from uninjured and thoracic level SCI mice. *C*: glomerular fibrosis score summary graph showing a similar level of fibrosis in kidneys from uninjured and SCI mice. Fibrosis score in the cortex (*D*) and medulla (*E*) of kidneys from uninjured and SCI mice. Although fibrosis scores were similar 24 h after injury, they trended higher at least in T3Tx injury mice at 4 wk postinjury and were more prominent in the medulla. Values are means ± SE. Statistical significance was determined by mixed model two-way ANOVA followed by Newman–Keuls post hoc tests for comparisons with uninjured control and injured mice at the indicated time points.

T10Tx SCI mice was relatively low (~1 AD event per animal over the 24-h recording period) and remained unchanged, the number of naturally occurring AD events progressively increased in T3Tx SCI mice starting 2 wk after injury and averaged ~10 AD events per day at 4 wk after T3Tx SCI.

Chronic High Thoracic-Level SCI Exacerbates Renal Injury

Previous studies have established a close association between SCI and renal dysfunction, partly attributable to the

Table 1. *Gravimetric data of adult uninjured female mice and their thoracic-level SCI cohorts*

	Control			T3tx SCI						T10tx SCI					
				24 h			4 wk			24 h			4 wk		
	n	Mean	SD	*n*	Mean	SD	*n*	Mean	SD	*n*	Mean	SD	*n*	Mean	SD
Body weight, g	7	21.59	1.06	4	24.68	1.26	8	17.84	0.51	3	22.73	0.42	8	20.48	0.58
Kidney weight, mg	7	140.29	9.02	4	203.25	7.80	8	127.75	7.23	3	207.00	7.03	8	148.03	8.42
Heart weight, mg	7	138.43	5.67	4	182.00	8.26	8	107.88	4.61	3	147.67	5.55	8	122.56	9.14
Kidney weight/body weight, μg/g	7	6.51	0.28	4	8.28	0.25	8	7.17	0.36	3	9.13	0.47	8	7.22	0.31
Heart weight/body weight, μg/g	7	6.47	0.30	4	7.54	0.76	8	6.09	0.30	3	6.51	0.36	8	5.96	0.36
Kidney weight/heart weight, μg/g	7	1.02	0.06	4	1.13	0.11	8	1.20	0.07	3	1.40	0.05	8	1.25	0.08

SCI, spinal cord injury; T3Tx, spinal cord transection at thoracic level 3; T10Tx, spinal cord transection at thoracic level 10.

renal effects of the ensuing hypotension and dysregulated sympathetic activity from the loss of supraspinal control of autonomic input to the kidney (4, 12). However, heretofore, it was unknown how SCI-induced hypotension in the acute phase and the ensuing bouts of extreme hypertension from AD in the chronic phase of the injury affect the structure and function of the kidney. To address these questions, we analyzed urine samples and histological sections of kidneys from T3Tx and T10Tx SCI mice 24 h and 4 wk after injury. As shown in Fig. 4*A*, urine protein excretion fell precipitously 24 h after both T3Tx and T10Tx injury relative to uninjured control and remained at low levels throughout the monitoring period. In contrast, urine creatinine excretion increased sharply shortly after injury and remained chronically elevated; at 3 and 4 wk postinjury, urine creatinine excretion trended higher in mice with T3Tx SCI relative to those with T10Tx SCI (Fig. 4*B*). Similar to urine protein levels, urine microalbumin excretion was markedly reduced 24 h after injury and remained suppressed at 4 wk in both T3Tx and T10Tx SCI mice (Fig. 4*C*). The renal injury marker NGAL was sharply elevated 24 h postinjury in both T3Tx and T10Tx SCI mice but decreased to baseline level in T10Tx SCI mice 4 wk after injury (Fig. 4*D*). To determine whether increased NGAL was associated with structural damage to the kidney, we assessed the level of tissue fibrosis using Masson's trichrome histological staining. Overall, SCI led to increased renal interstitial fibrosis, which was more prominent at 4 wk postinjury (Fig. 5, *A* and *B*). Fibrosis in the renal cortex trended equally higher in both groups of SCI mice at 4 wk postinjury, whereas medullary fibrosis was markedly elevated only in T3Tx SCI mice at the same time point (Fig. 5, *D* and *E*). The glomerular fibrosis score was similar between kidneys from uninjured control and SCI mice (Fig. 5*B*). At 4 wk postinjury, T3Tx SCI mice showed decreased body weight (Table 1). The kidney weight-to-body weight ratio trended higher in both groups of SCI mice 24 h after injury but returned to a similar level as in uninjured control mice 4 wk after injury.

High Thoracic-Level SCI Impairs Autoregulation of RBF

To investigate the pathophysiological mechanisms that mediate renal injury following thoracic-level SCI, we determined the extent to which SCI affects renal hemodynamics and autoregulation to alter renal perfusion. To this end, we assessed the renal hemodynamic response to a sudden increase in systemic pressure in SCI mice 24 h and 4 wk after T3Tx or T10Tx and compared with the response in uninjured animals. Consistent with the telemetry results shown in Fig. 1, absolute baseline SBP and RBF under isoflurane anesthesia were substantially reduced in T3Tx but not T10Tx SCI mice at 24 h and 4 wk postinjury (Table 2). In all groups, simultaneous occlusion of the celiac and superior mesenteric arteries under anesthesia caused an ~20-mmHg increase in SBP (Fig. 6*A*, *top* graphs); however, absolute SBP remained reduced in T3Tx SCI mice (Table 2). In uninjured mice, the rise in systemic pressure led to a rapid fall in RBF and a rise in RVR (Fig. 6*A*, *middle* and *bottom* graphs). At the nadir or peak of the response to increased SBP, absolute RBF trended lower, whereas RVR trended higher, in T3Tx SCI mice at 24 h postinjury; conversely, RBF appeared elevated, whereas RVR was reduced, in the same group relative to uninjured or T10Tx SCI mice at 4 wk postinjury (Tables 3 and 4). The patterns of RBF and the RVR response to an increase in systemic pressure were similar between uninjured and SCI mice 24 h postinjury except that the magnitude of the fall in RBF was lessened, whereas the RVR response was exaggerated, in T3Tx SCI mice. However, at 4 wk postinjury, and in contrast

Table 2. *Absolute blood pressure values before and after the administration of ANG II, NE, or concurrent occlusion of the celiac and superior mesenteric arteries in uninjured, T3Tx, and T10Tx female mice 24 h or 4 wk after injury*

Injury Level/Treatment	24 h After SCI			4 wk After SCI		
	Uninjured (*n* = 7)	T3Tx (*n* = 3–7)	T10Tx (*n* = 3–8)	Uninjured (*n* = 7)	T3Tx (*n* = 5–8)	T10Tx (*n* = 5–8)
Baseline	80 ± 6	59 ± 2[c]	87 ± 4[f]	80 ± 6	67 ± 5	83 ± 5
NE (10 μg/kg)	119 ± 4	101 ± 7[b]	113 ± 2[d]	119 ± 4	93 ± 5[b]	110 ± 7[d]
Baseline	90 ± 3	61 ± 1[c]	89 ± 3[f]	90 ± 3	68 ± 5[a]	86 ± 5[d]
ANG II (1 μg/kg)	111 ± 4	83 ± 3[c]	102 ± 3[e]	111 ± 4	82 ± 7[b]	99 ± 6[d]
Baseline	82 ± 5	65 ± 7[b]	83 ± 1[d]	82 ± 5	59 ± 4[a]	87 ± 3[f]
Carotid and superior mesenteric artery occlusion	108 ± 4	85 ± 6[b]	105 ± 3[d]	108 ± 4	75 ± 5[c]	105 ± 4[f]

All values are means ± SE (in mmHg). [a]$P < 0.05$, [b]$P < 0.01$, and [c]$P < 0.001$ vs. uninjured mice; [d]$P < 0.05$, [e]$P < 0.01$, and [f]$P < 0.001$ vs. T3Tx mice. ANG II, angiotensin II; NE, norepinephrine; SCI, spinal cord injury; T3Tx, spinal cord transection at thoracic level 3; T10Tx, spinal cord transection at thoracic level 10.

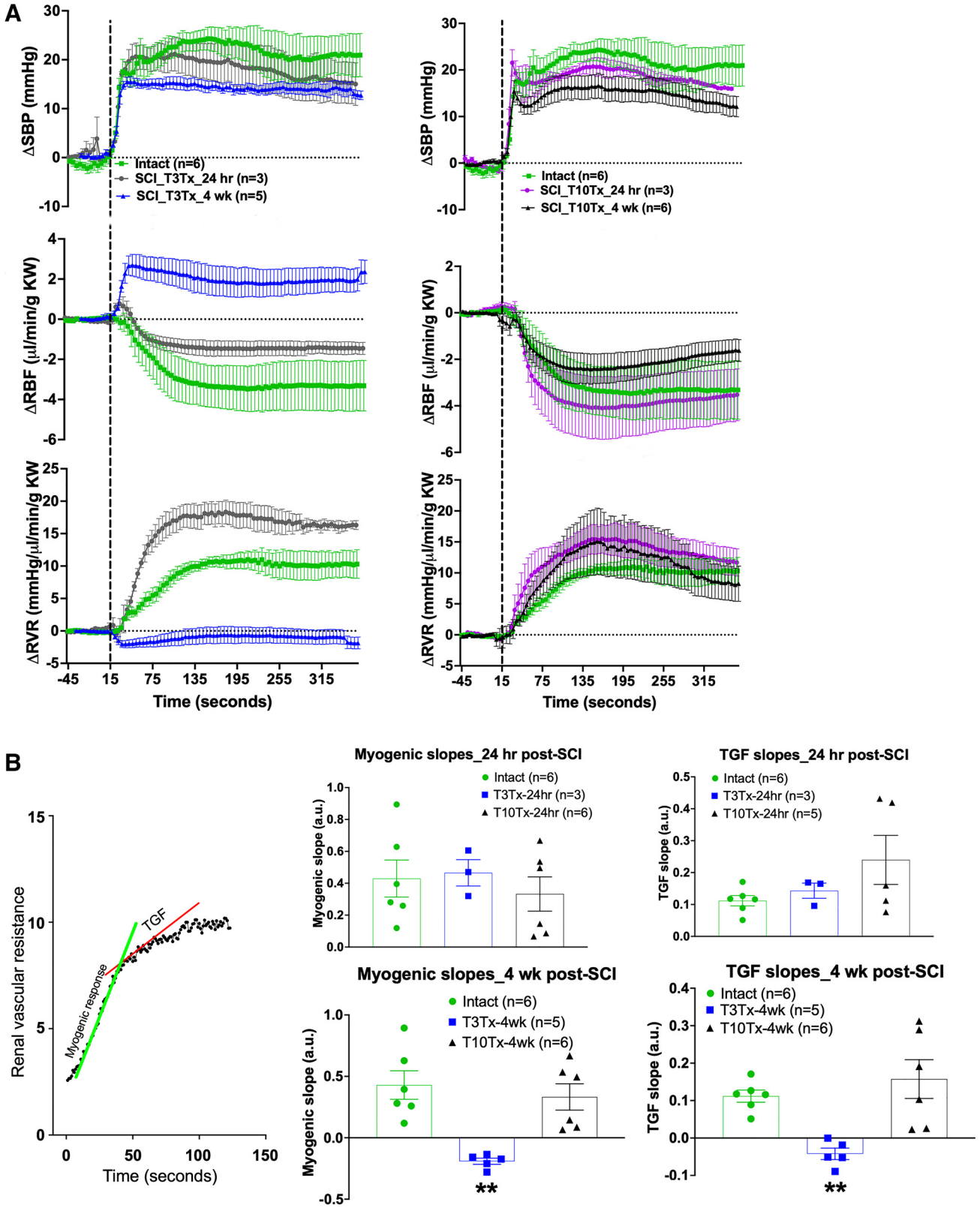

to the response profiles at 24 h after injury, RBF and RVR responses were inverted, i.e., RBF increased whereas RVR decreased, following a similar level of a step increase in systemic pressure (Fig. 6*A*). The inversion of the RBF and RVR response patterns was unique to T3Tx SCI mice as the response patterns in T10Tx SCI mice at 24 h or 4 wk were similar to those of uninjured or T3Tx SCI mice at 24 h postinjury. These observations then led us to determine whether the

Table 3. *Absolute renal blood flow values before and after the administration of ANG II, NE, or concurrent occlusion of the celiac and superior mesenteric arteries in uninjured, T3Tx, and T10Tx female mice 24 h or 4 wk after injury*

Injury Level/Treatment	24 h After SCI			4 wk After SCI		
	Uninjured (n = 7)	T3Tx (n = 3–7)	T10Tx (n = 3–8)	Uninjured (n = 7)	T3Tx (n = 5–8)	T10Tx (n = 5–8)
Baseline	7.7 ± 1.3	4.5 ± 1.2	5.6 ± 1.4	7.7 ± 1.3	6.3 ± 0.7	6.8 ± 1.6
NE (10 μg/kg)	4.2 ± 0.4	4.1 ± 1.0	3.7 ± 0.7	4.2 ± 0.4	6.7 ± 0.8	5.4 ± 1.1
Baseline	6.6 ± 1.6	5.6 ± 1.5	5.0 ± 0.3	6.6 ± 1.6	5.8 ± 0.7	6.5 ± 1.5
ANG II (1 μg/kg)	2.5 ± 0.5	3.0 ± 1.0	2.6 ± 0.4	2.5 ± 0.5	5.6 ± 0.6	4.8 ± 1.0
Baseline	8.4 ± 1.2	3.4 ± 0.7*	8.2 ± 2.1†	8.4 ± 1.2	4.8 ± 0.3	7.8 ± 1.9
Carotid and superior mesenteric artery occlusion	5.1 ± 0.3	3.1 ± 1.2	4.5 ± 0.8	5.1 ± 0.3	7.7 ± 0.6	5.4 ± 1.4

All values are means ± SE (in μL/min/g kidney wt). *$P < 0.01$ vs. uninjured mice; †$P < 0.05$ vs. T3Tx mice. ANG II, angiotensin II; NE, norepinephrine; SCI, spinal cord injury; T3Tx, spinal cord transection at thoracic level 3; T10Tx, spinal cord transection at thoracic level 10.

drastic change in the renal hemodynamic response to increased systemic pressure after high thoracic-level SCI involved any change in the sensitivity or efficiency of the mechanisms underlying renal autoregulation, i.e., the myogenic response and TGF. As shown in Fig. 6*B*, we did not observe any change in the sensitivity of the myogenic response and TGF (as determined, respectively, by the slope of the initial sharp rise and the later slower rise in the RVR response to increased systemic pressure) in SCI mice at 24 h postinjury relative to uninjured animals. However, in T3Tx SCI mice, the sensitivity of the myogenic response and TGF was inverted at 4 wk postinjury, whereas the same parameters in T10Tx SCI mice were similar to those of uninjured animals.

The RBF Response to NE and ANG II-Induced Rise in Systemic Pressure Is Attenuated After High Thoracic-Level SCI

To further explore the physiological mechanisms underlying impaired renal hemodynamics following high thoracic-level SCI, we examined the renal hemodynamic response to systemic pressure increase by a bolus intravenous administration of the sympathetic neurotransmitter NE or ANG II under isoflurane anesthesia. In uninjured mice, NE injection increased SBP by ~40 mmHg, accompanied by a rapid fall in RBF and a concomitant rise in RVR. In injured mice, NE induced a pressor response but at a lower magnitude in T3Tx 24-h SCI mice relative to uninjured and T10Tx mice (Fig. 7*A*, *top* graphs). In contrast to the response in uninjured and T10Tx SCI mice, RBF in T3Tx SCI mice, at either 24 h or 4 wk after injury, increased in response to the rise in SBP after NE injection (Fig. 7*A*, *middle* graphs), whereas the rise in RVR was attenuated at 4 wk in this group (Fig. 7*A*, *bottom* graphs). In T10Tx mice, RBF and RVR response to NE-induced increase in SBP was similar to uninjured controls. Despite the pressor effect of NE, absolute SBP remained low, whereas RBF trended high in T3Tx mice at 4 wk postinjury (Table 3). Conversely, RVR after NE administration trended higher in both groups of SCI mice relative to uninjured mice at 24 h postinjury; however, RVR appeared low in T3Tx mice relative to uninjured and T10Tx SCI mice at 4 wk postinjury (Table 4). ANG II administration evoked similar response patterns as NE in uninjured and SCI mice except that the rise in RBF in T3Tx mice was replaced by a mild drop in the response (Fig. 7*B*). Moreover, the RVR response to ANG II was suppressed in both T3Tx and T10Tx SCI at 4 wk after injury (Fig. 7*B*, *bottom* graphs). Interestingly, absolute RBF was very similar after ANG II administration in all groups at 24 h postinjury, whereas at 4 wk postinjury, it trended higher in both groups of SCI mice (Table 3). In contrast to the levels after NE administration, RVR was robustly elevated by ANG II in uninjured and T3Tx mice relative to T10Tx mice; however, at 4 wk after SCI, ANG II caused a modest increase in RVR in T3Tx SCI mice relative to uninjured or T10Tx SCI mice (Table 4).

Impaired Renal Autoregulation After High Thoracic-Level SCI Is Accompanied by Elastin Fragmentation and Collagen Deposition in and Around the Kidney Microvasculature

To determine whether renal hemodynamic impairment during chronic SCI is associated with structural changes in the renal microvasculature, we performed histological staining and analysis of elastin fiber organization and collagen deposition in and around small intrarenal arteries as well as glomerular collagen deposition and red blood cell content. Fragmentation of the elastic laminae in small renal arteries was visible 24 h after either T3Tx or T10Tx and worsened more remarkably in the chronic phase of T3Tx injury (Fig. 8*A*). After either T3Tx or T10Tx SCI, collagen

Figure 6. High-level spinal cord injury (SCI) impairs the renal autoregulatory response to increased perfusion pressure. *A*: time course of changes in renal blood flow (RBF) and renal vascular resistance (RVR) following a step increase in systemic blood pressure under isoflurane anesthesia. Systolic blood pressure (SBP) was raised by simultaneously tying the celiac and superior mesenteric arteries, thereby occluding them and redirecting more blood to the renal arteries to increase renal perfusion pressure (RPP). The dashed line represents the time of occlusion of the celiac and superior mesenteric arteries. In uninjured animals, increasing RPP caused a precipitous drop in RBF and increased RVR. This phenomenon was recapitulated in spinal cord transection at thoracic level 3 (T3Tx) and thoracic level 10 (T10Tx) SCI animals 24 h after injury, although it was less pronounced in T3Tx 24-h mice. In contrast, RBF and RVR response to increased RPP was reversed in T3Tx animals 4 wk after SCI, whereas the response in T10Tx animals was similar to that of uninjured mice. *B*: summary of the sensitivity of the myogenic response and tubuloglomerular feedback (TGF) response to a step increase in RPP. Sensitivity was determined by the slope of the initial and late phase rise in RVR as shown in the line graph schematic on the *left*. Values are means ± SE. Statistical significance was determined by mixed model two-way ANOVA followed by Dunnett's post hoc tests for comparisons with uninjured control at the indicated time points. **$P < 0.01$ vs. uninjured control. KW, kidney weight.

Table 4. *Absolute renal vascular resistance values before and after the administration of ANG II, NE, or concurrent occlusion of the celiac and superior mesenteric arteries in uninjured, T3Tx, and T10Tx female mice 24 h or 4 wk after injury*

Injury Level/Treatment	24 h After SCI			4 wk After SCI		
	Uninjured (n = 7)	T3Tx (n = 3–7)	T10Tx (n = 3–8)	Uninjured (n = 7)	T3Tx (n = 5–8)	T10Tx (n = 5–8)
Baseline	12 ± 2	23 ± 7	21 ± 6	12 ± 2	12 ± 2	22 ± 7
NE (10 μg/kg)	29 ± 3	42 ± 14	35 ± 7	29 ± 3	18 ± 3	36 ± 12
Baseline	16 ± 3	17 ± 5	23 ± 6	16 ± 3	13 ± 0	23 ± 7
ANG II (1 μg/kg)	52 ± 13	54 ± 17	44 ± 6	52 ± 13	16 ± 2†	36 ± 12‡
Baseline	11 ± 2	17 ± 3	12 ± 4	11 ± 2	12 ± 1	19 ± 7
Carotid and superior mesenteric artery occlusion	24 ± 2	36 ± 3	28 ± 7	24 ± 2	10 ± 1	35 ± 13*§

All values are means ± SE (in mmHg/μL/min/g kidney wt). *$P < 0.05$ and †$P < 0.01$ vs. uninjured mice; ‡$P < 0.05$, and §$P < 0.01$ vs. T3Tx mice. ANG II, angiotensin II; NE, norepinephrine; SCI, spinal cord injury; T3Tx, spinal cord transection at thoracic level 3; T10Tx, spinal cord transection at thoracic level 10.

content within the medial layer of the intrarenal arteries increased in the acute phase and was enhanced in the chronic phase (Fig. 8*B*, *left* graph). In contrast, perivascular collagen deposition was enhanced only in the chronic phase and was more robust in T3Tx intrarenal arteries (Fig. 8*B*, *right* graph). Similarly, glomerular collagen deposition was markedly increased in the chronic phase of injury and was more remarkable after T3Tx injury (Fig. 8, *C* and *D*). Glomerular congestion, determined by the level of red blood cells in the renal corpuscle, was augmented 24 h after T10Tx injury; however, it was elevated during the chronic phase of both injury levels (Fig. 8, *C* and *E*).

Thoracic SCI Stimulates Differential Expression of Genes Involved in ECM Modification and Proinflammatory Cytokine Signaling in the Kidney

We performed transcriptomic analysis by unbiased bulk sequencing of RNA extracted from the kidneys of female SCI mice to identify potential mechanisms, at the molecular level, that likely mediate the differences in renal hemodynamics and injury outcomes observed at 4 wk following T3Tx and T10Tx SCI. We identified 2,660 differentially expressed genes (with a fold-change of >0.6, $P < 0.05$) of 15,676 genes with measured expression in kidney samples from T3Tx SCI mice, in contrast to 2,278 differentially expressed genes of 15,622 genes with measured expression in T10Tx SCI kidney samples (Fig. 9*A*). From pathway analysis, we found that genes in cytokine-cytokine receptor interactions were most perturbed in both T3Tx and T10Tx SCI kidneys, whereas perturbation of the chemokine signaling pathway was found only in T3Tx SCI relative to uninjured samples (Fig. 9*B*). GO analysis for cellular components and biological processes revealed enrichment of genes involved in the extracellular space/region and adaptive and humoral immune responses as the highest and most relevant to the effects of SCI on the structure and function of the kidney (Fig. 9*C* and Supplemental Tables S1–S4; all Supplemental material is available at https://doi.org/10.6084/m9.figshare.19379978.v1). Among the biological processes with highly significant GO enrichment, a total of 398 of 1,838 genes were differentially expressed in T3Tx SCI samples whereas 137 of 511 genes were differentially expressed in T10Tx SCI samples, each relative to uninjured control samples. Next, we used real-time PCR to determine the relative expression of candidate genes involved in ECM remodeling and the inflammatory response and that showed high enrichment in the GO. We used RNA from uninjured kidney samples and from SCI mice at 24 h and 4 wk after injury. Figure 10 shows that among the three ECM modifying genes examined, including *Mmp3*, *Adamts1*, and *Adamts4*, only *Mmp3* showed an appreciable increase in expression in both groups of SCI samples, reaching statistical significance only in T3Tx SCI samples at 24 h postinjury. This was accompanied by a marked increase in *Col13a1* expression at 24 h postinjury in T3Tx SCI samples. Among the cytokines examined by quantitative PCR, only *Cxcl10* showed increased expression at 4 wk postinjury in the T3Tx SCI group, whereas *Vegfa*, *Il6*, and *Il11* as well as the marker of acute inflammation *Saa1* all showed an increasing trend that was not statistically significant at either 24 h or 4 wk postinjury. We then measured secreted plasma levels of IL-6 and SAA1 collected 24 h or 4 wk after SCI to assess whether the global inflammatory response to SCI was altered by the level of thoracic injury. As shown in Fig. 11*A*, there was a marked increase in the plasma SAA1 level, which remained significantly elevated 4 wk after T3Tx or T10Tx SCI. Serum IL-6 was elevated within 24 h of T3Tx or T10Tx SCI and decreased to the uninjured level 4 wk after injury (Fig. 11*B*).

DISCUSSION

Renal dysfunction is an established contributor to urinary complications, including excessive urine production during bed rest and sleep, in the chronic phase of SCI. However, the mechanisms mediating SCI-induced renal dysfunction are poorly understood. In this study, we explored the acute and chronic effects of complete high (i.e., T3) and low (i.e., T10) thoracic-level SCI on the structure and function of the kidney. By examining renal hemodynamics, we show that high thoracic-level transection SCI causes failure of the autoregulatory response of the renal vasculature to increased perfusion pressure and a decline in the responsiveness of RBF to vasoactive agents, including NE and ANG II. These functional alterations are accompanied by structural changes in the renal parenchyma and vasculature, including interstitial, intravascular, and perivascular fibrosis, and fragmentation of vascular elastic laminae accompanied by differential expression of genes involved in ECM remodeling.

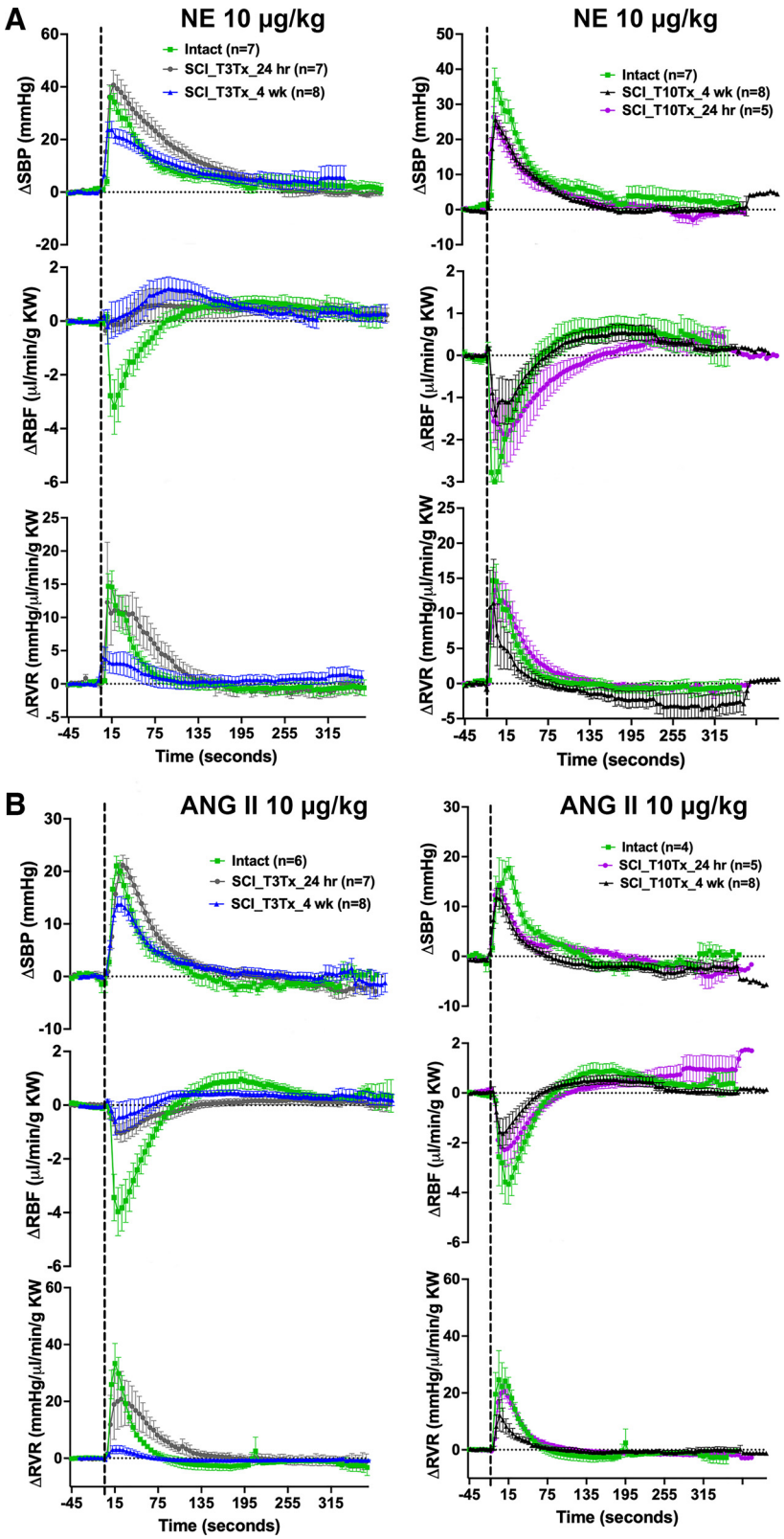

Figure 7. High thoracic-level spinal cord injury (SCI) impairs renal hemodynamic response to agonist-induced increases in systemic pressure. *A*: time course of changes in renal blood flow (RBF) and renal vascular resistance (RVR) following a bolus administration of norepinephrine (NE; 10 µg/kg iv) or angiotensin II (ANG II; 1 µg/kg iv) under isoflurane anesthesia. The dashed line represents the time of agonist administration. In uninjured animals, increasing systolic blood pressure (SBP) with NE caused a precipitous drop in RBF while increasing RVR. This phenomenon was recapitulated in spinal cord transection at thoracic level 10 (T10Tx) SCI animals but markedly attenuated in spinal cord transection at thoracic level 3 (T3Tx) SCI animals, more noticeably at 4 wk after injury. *B*: time course of changes in RBF and RVR following a bolus administration of angiotensin II (ANG II; 1 µg/kg iv). The dashed line represents the time of agonist administration. As was seen following NE administration, the RBF response to an ANG II-induced increase in SBP was markedly attenuated in T3Tx SCI mice, although RVR increased as in uninjured mice at 24 h after injury. However, the RVR response was suppressed in both SCI groups at 4 wk after injury. Values are means ± SE.

SCI induces marked changes in the circulatory and thermoregulatory systems; this has been well established by several studies (12, 45–48). We confirmed such SCI-triggered responses, including profound hypotension, bradycardia, and hypothermia, by continuous monitoring of systemic hemodynamics and body temperature. We also observed that the duration and recovery of the marked changes in systemic hemodynamics and body temperature depend on the level of thoracic spinal cord transection/injury. Following T10Tx SCI, hemodynamic parameters and body temperature

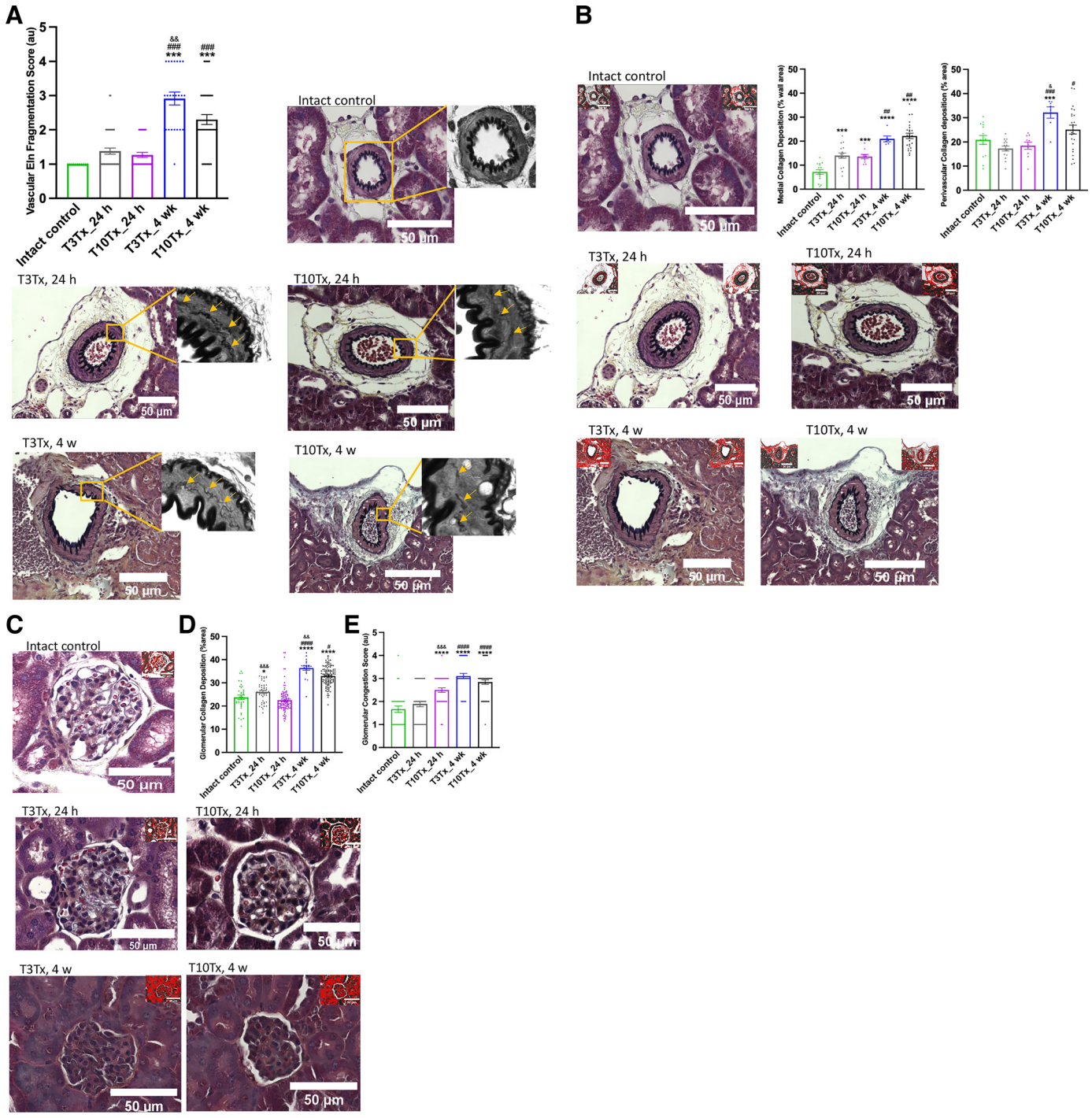

return to pretransection levels just 1 h postinjury. In contrast, the recovery of the same parameters is prolonged after T3Tx SCI, and only SBP rises close to the preinjury level whereas HR and body temperature remain suppressed. These SCI level-associated differences in the profiles of systemic hemodynamics and body temperature recovery may be attributable to the degree of disrupted supraspinal control of autonomic—largely sympathetic—input. Whereas T3Tx SCI completely disrupts all supraspinal input to preganglionic nerves in the thoracic (T10–T12) and lumbar (L1–L3) sympathetic trunks of the intermediolateral cell column, T10Tx SCI completely disrupts projections only to the lumbar sympathetic preganglionic nerves (L1–L3) while possibly sparing some projections to preganglionic nerves emanating from the T10–T12 sympathetic trunk, thereby facilitating the reestablishment of basal sympathetic drive. Such a level-dependent disruption of supraspinal control of sympathetic input to the kidney could lead either to uncontrolled release or excessive withdrawal of local sympathetic neurotransmission. Either scenario could lead to desensitization or supersensitivity of adrenergic receptors in the renal vasculature, thereby affecting the RVR response to

exogenous agonists. In this study, the RVR response in T3Tx mice at 24 h postinjury appeared the most robust compared with T10Tx or uninjured animals, which is consistent with decreased renal sympathetic neurotransmission, likely resulting in receptor supersensitivity and augmented vasoconstriction, at least in the acute phase of the injury and before any (mal)adaptive remodeling.

The slow rate of recovery of blood pressure, HR, and body temperature also suggests a shift from dependence on sympathetic activity to a new hormonal system, such as the renin-angiotensin-aldosterone system (RAAS), to maintain hemodynamic and temperature homeostasis. The RAAS raises blood pressure by increasing peripheral vascular resistance via the contractile action of ANG II in the vasculature; it also increases extracellular fluid volume and thus cardiac output by stimulating tubular Na^+ and water reabsorption (49). The precipitous fall in blood pressure after SCI is known to be associated with a robust increase in the activity of plasma renin, the rate-limiting enzyme of the RAAS (50). Increased renin activity after SCI has been attributed to renal baroreceptor-mediated renin release stimulated by the marked fall in systemic blood pressure causing afferent arteriolar dilatation (51). In this study, the gradual rise in blood pressure could, therefore, be attributed to RAAS-dependent fluid retention and vasoconstriction resulting from accumulating ANG II and aldosterone. In addition, chronically elevated RAAS activity could decrease the sensitivity of the renal vasculature to an acute surge in ANG II as occurs with intravenous administration. Indeed, the RVR response to bolus ANG II administration was remarkably reduced in the chronic phase of T3Tx SCI compared with the response in the acute phase of the injury, consistent with receptor desensitization. The result is also consistent with the hypothesis that persistent hypotension after high thoracic-level SCI might trigger a sustained elevation of the RAAS. Both T3Tx and T10Tx also abolish the circadian rhythm of blood pressure, HR, and body temperature in the first 24 h, resuming 1 wk postinjury. This observation is consistent with previous studies suggesting that the circadian rhythm is controlled by a pathway linking central nervous system centers to spinal preganglionic neurons below T3 and that the disruption of such a pathway by SCI may be temporary (46, 52).

Previous studies have shown alterations in renal function during the acute phase of high and low thoracic-level injury (12, 13); however, the effects on structural changes in the kidney were not explored. Consistent with those findings (12), we show in this study that both high and low thoracic-level SCI cause a sharp decline in urine protein and albumin excretion within 24 h of injury, indicating a marked drop in renal perfusion and GFR in the acute phase of injury. In the weeks following injury, urine protein excretion gradually increases, paralleled by a similar trend in the recovery of systemic pressure towards preinjury baseline levels. The gradual increase in systemic pressure also likely increases RPP and GFR, thereby increasing total urine protein excretion. Contrary to proteinuria, urine creatinine excretion sharply increases 24 h after injury and continues to rise in the chronic phase. This is consistent with the widely observed weight loss following SCI, as food and water consumption declines and muscle atrophy increases (53–55). Of note, heart weight and kidney weight increase in the acute phase, which is likely due to fluid retention as blood pressure and the circulatory system are severely impaired. Over time, and as systemic hemodynamics improved, kidney weight and heart weight returned to uninjured control levels in T10Tx animals. In T3Tx mice, however, these values remained below control levels. These observations are consistent with a recent report showing cardiac atrophy during the chronic phase of T3 transection in mice (56). Injury at both high and low thoracic levels led to the elevation of the renal injury marker NGAL in the urine during the acute phase. At 4 wk postinjury, urine NGAL returned to the preinjury level in T10Tx animals but not T3Tx animals. This may be due to T3Tx animals experiencing multiple, daily episodes of hypertensive AD during chronic injury (57). This observation is consistent with the renal interstitial fibrosis that was more prominent in the renal medulla of T3Tx mice in the chronic phase of the injury. Together, these results indicate that impairment of renal function following SCI is accompanied by structural damage to the kidney, and the severity of such damage is dependent on injury level.

A remarkable observation we made in this study is that, very shortly after T3Tx, the dynamic response of RVR to a step increase in systemic pressure was exaggerated, whereas in the chronic phase, it was almost completely abolished, thereby causing RBF to increase instead of decrease in response to elevated RPP. The exaggerated RVR response in the acute phase could be due to sustained RAAS activation

Figure 8. Structural changes in the renal vasculature and glomerulus resulting from spinal cord injury (SCI) are enhanced after high thoracic spinal transection. *A*: representative images and a summarized bar graph of Movat histological staining showing the level of elastic lamina fragmentation in small intrarenal arteries. Yellow arrows in the grayscale *insets* indicate fragmented elastin in the medial layer of the vessel wall. Vascular elastic lamina fragmentation was scored using an arbitrary scale of 1–5 (where 1 = little to no elastic lamina breaks and 5 = multiple discontinuity of the elastic lamina, including in the internal and external elastic laminae. *B*: representative images and summarized bar graphs of Movat staining showing collagen deposition in the medial layer of intrarenal arteries and in the perivascular space. Collagen content was measured using the K-means clustering method to generate color-segmented copies of the original histological images. ImageJ was then used to split the images into red, green, and blue channels to obtain the best contrast of extracellular matrix components in the regions of interest. The area of collagen highlighted red was then measured and expressed as a percentage of the vessel wall area (medial collagen deposition) or total area of the perivascular region (perivascular collagen deposition). Data were pooled from at least 8 vessels from 3 animals for each group. *C*: representative histological images of glomeruli in unperfused kidneys with Movat staining showing the presence of red blood cells (RBC) and collagen deposition. Collagen deposition was assessed as described above, whereas glomerular congestion was scored on a scale of 1–5 (where 1 = little to no visible RBC and 5 = overt RBC accumulation in the corpuscle). *D*: summary bar graph of glomerular collagen deposition expressed as a percentage of the total glomerular area. *E*: summary bar graph of glomerular congestion. Values are means ± SE. Statistical significance was determined by ordinary one-way ANOVA followed by Newman–Keuls post hoc tests for comparisons. ****$P < 0.0001$ and ***$P < 0.001$ vs. uninjured control; ####$P < 0.0001$, ###$P < 0.001$, ##$P < 0.01$, and #$P < 0.05$ vs. 24 h after the same injury level; &&&$P < 0.001$, &&$P < 0.01$, and &$P < 0.05$ vs. T10Tx at the same time point after injury. au, arbitrary units; T3Tx and T10Tx, spinal cord transection at thoracic level 3 (T3) and thoracic level 10 (T10), respectively.

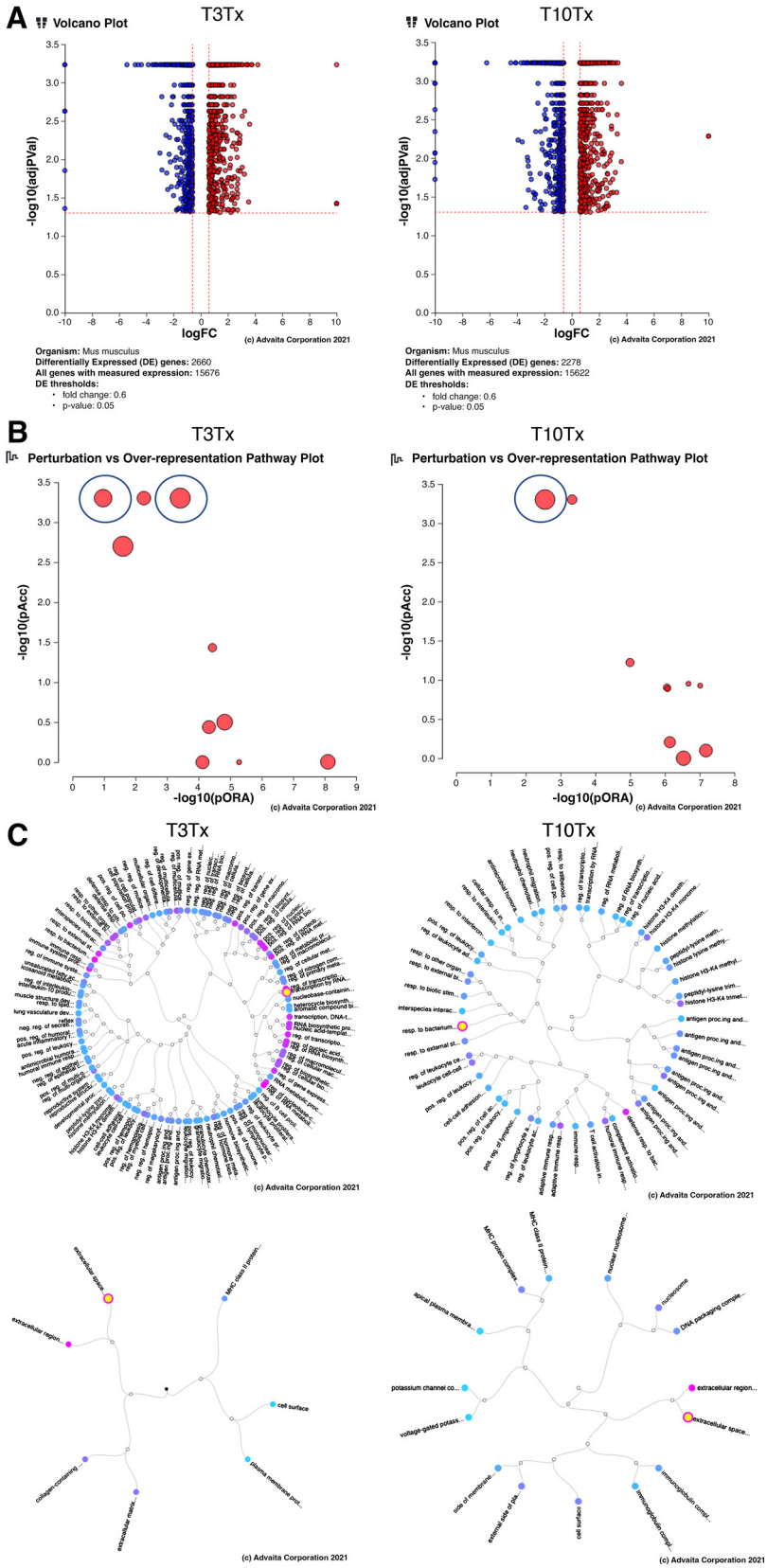

Figure 9. Thoracic spinal cord injury (SCI) induces transcriptional responses in the kidney. *A*: volcano plots of bulk RNA-sequencing data showing profiles of genes differentially expressed among all measured genes in kidney samples obtained from uninjured control mice (n = 3), spinal cord transection at thoracic level 3 (T3Tx) SCI mice (n = 3), and spinal cord transection at thoracic level 10 (T10Tx) SCI mice (n = 3) at 4 wk postinjury. *B*: scatterplots of pathway analysis showing the top 10 overrepresented pathways that were significantly perturbed. The blue-circled red dots in the intact versus T3Tx plot (*left*) are cytokine-cytokine receptor and chemokine signaling pathways; the only circled red dot in the intact versus T10Tx plot (*right*) represents a cytokine-cytokine receptor signaling pathway. *C*: dendrograms from Gene Ontology analysis showing terms of biological processes (*top*) and cellular components (*bottom*) with high enrichment of member gene sets.

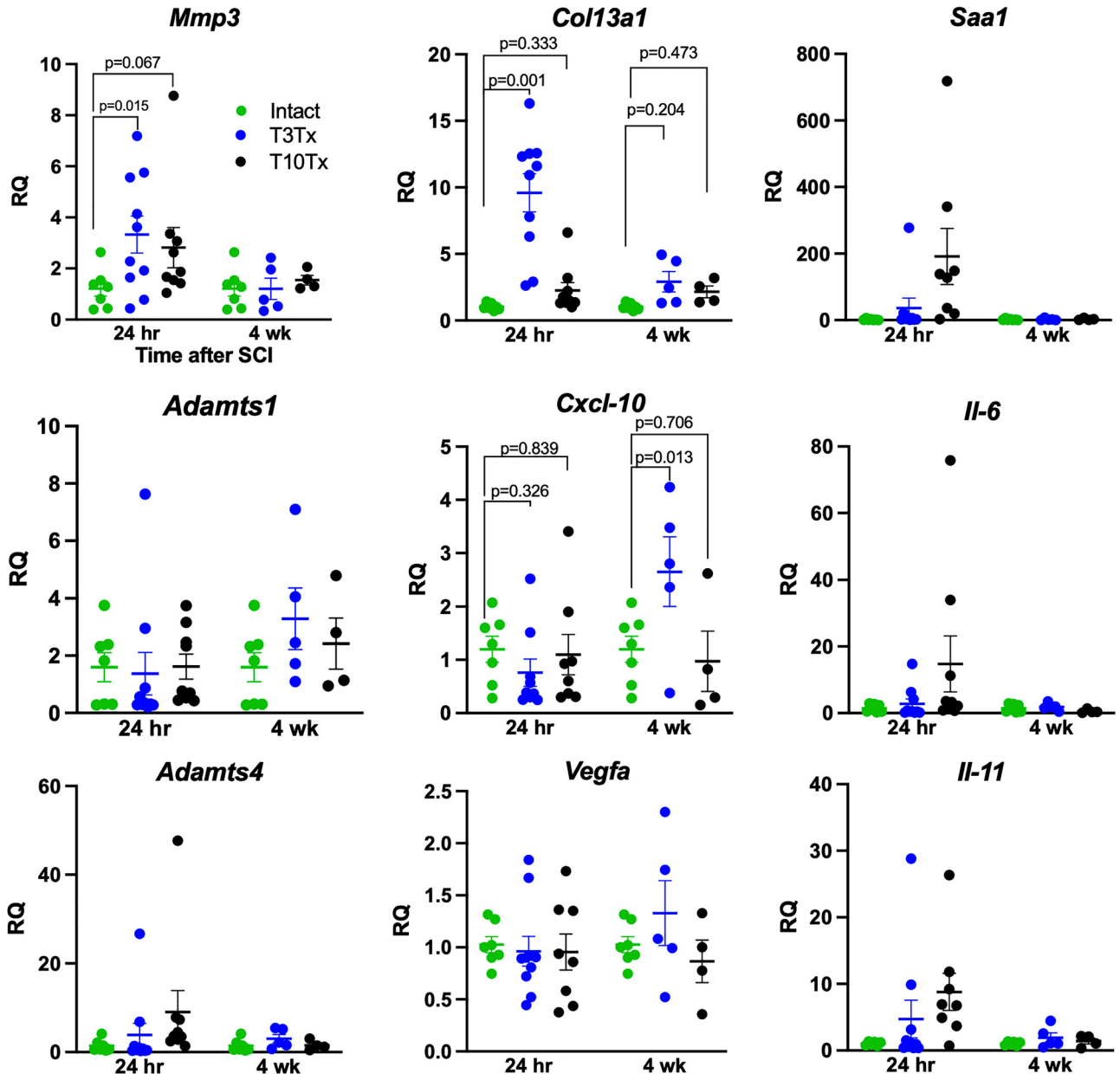

Figure 10. Thoracic spinal cord injury (SCI) induces the expression of genes involved the inflammatory response and extracellular matrix modification. Gene expression in kidney samples harvested 24 h and 4 wk in uninjured mice as well as from spinal cord transection at thoracic level 3 (T3Tx) and thoracic level 10 (T10Tx) SCI mice was assessed using two-step real-time PCR. The fold-change in gene expression was determined using the $\Delta\Delta C_t$ method (where C_t is threshold cycle). During the acute phase (24 h postinjury), the expression of matrix metalloproteinase-3 (*Mmp3*) and collagen type XIII-α_1 (*Col13a1*) was significantly increased in kidneys from T3Tx SCI mice relative to intact uninjured mice. In the chronic phase (4 wk postinjury), the expression of chemokine (C-X-C mofit) ligand 10 (*Cxcl10*) was augmented in kidneys from T3Tx SCI mice relative to intact uninjured mice. RQ is the fold-change in gene expression normalized to *Gapdh* and relative to normalized expression in samples from uninjured mice. *Adamts1*, ADAM metallopeptidase with thrombospondin type 1 motif 1; *Adamts4*, ADAM metallopeptidase with thrombospondin type 1 motif 4; *Il6*, interleukin-6; *Il11*, interleukin 11; *Saa1*, serum amyloid A1; *Vegfa*, vascular endothelial growth factor A.

triggered by the prolonged hypotension after T3Tx. Elevated circulatory level of ANG II from the activated RAAS could potentiate pressure-induced constriction of the renal microvasculature, including the afferent and efferent arterioles, which are particularly sensitive to ANG II (58–62). Sustained activation of the RAAS with elevated ANG II in the circulation could reduce the pressor and/or hemodynamic response to the administration of exogenous ANG II. In agreement with this suggestion, we found that RVR and RBF response to exogenous ANG II was diminished in T3Tx SCI animals. During the chronic phase of T3Tx, RVR was completely insensitive to changes in RPP. In addition, the response to exogenous ANG II was markedly diminished, suggesting an already elevated level of circulating ANG II from the activated RAAS. Sustained activation of the RAAS in chronic T3Tx SCI may cause diminished ANG II-dependent vasoconstriction as a result of refractoriness or desensitization of the cognate receptors and

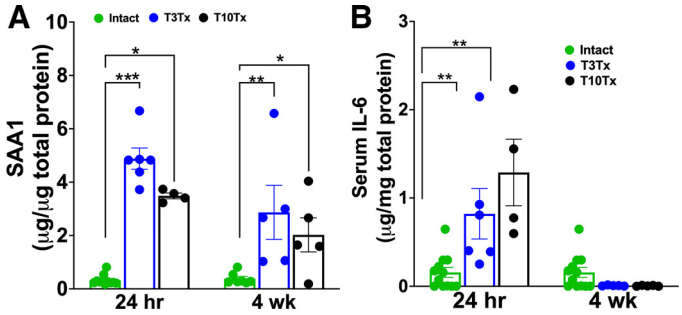

Figure 11. Thoracic spinal cord injury (SCI) elevates circulating levels of inflammatory cytokines. Plasma levels of serum amyloid A1 (SAA1) and interleukin-6 (IL-6) were measured. *A*: plasma SAA1 levels were elevated during acute (24 h) and chronic (4 wk) phases of spinal cord transection at thoracic level 3 (T3Tx) and thoracic level 10 (T10Tx) SCI compared with the level in uninjured controls. *B*: plasma levels of IL-6 were markedly increased after acute T3Tx and T10Tx injury but receded to a similar level in uninjured control in the chronic phase. ***$P < 0.001$, **$P < 0.01$, and *$P < 0.05$ vs. uninjured control.

downstream contractile signaling pathways. This phenomenon has been demonstrated in several vascular beds, such as in renal, carotid, iliac, and pulmonary arteries and the aorta (63, 64). For instance, acute ex vivo treatment of rat pulmonary arteries with ANG II has been shown to reduce plasma membrane expression of ANG II type 1 receptors for a prolonged period, thereby reducing its contractile effect (64). In addition, ANG II effects are terminated partly through angiotensin-converting enzyme 2-mediated cleavage to form ANG(1–7), which causes vasodilation by stimulating Mas receptors (65–68). Thus, an alternative mechanism accounting for the reduced pressor response to ANG II could be an increased circulating level and action of ANG (1–7). As our results show, the profile of the renal hemodynamic response during the acute or chronic phase also depends on the level of injury. In contrast to the response after T3Tx SCI, the renal hemodynamic response to changes in perfusion pressure, either by the application of vasoactive ligands or manual elevation of systemic pressure, after T10Tx was slightly altered or unaffected during the acute and chronic phases of SCI. This could be due to sparing of supraspinal control of preganglionic neurons at T10 or close to the area of spinal transection. As previously reported, mild or incomplete spinal crush injuries can indeed lead to adequate axonal sparing for maintaining normal cardiovascular regulation by supraspinal control of vasomotor pathways (69, 70). Similarly, a clean low thoracic-level spinal transection, as performed in T10Tx SCI, can lead to the preservation of sufficient supraspinal control of autonomic input to the kidney to facilitate the renal vascular response to changes in perfusion pressure. Sparing of supraspinal control of renal autonomic input after T10Tx could also maintain the regulation of the release of neurotransmitters and other factors for preserving vascular smooth muscle contractile phenotype and sensitivity to mechanical stimuli inducing myogenic constriction during chronic SCI, which would be absent in the chronic phase of T3Tx SCI.

Based on the finding that T3Tx exacerbates renal fibrosis, we hypothesize that maladaptation of the renal vascular bed to lower perfusion pressure contributes to renal autoregulation failure and impaired RVR and RBF responses to increased RPP after high thoracic-level SCI. As revealed by the histological examination, both T3Tx and T10Tx SCI caused glomerular, medial, and perivascular deposition of collagen and fragmentation of vascular elastic lamina in the chronic phase of spinal injury. These observations agree with the robust renal interstitial fibrosis after T3Tx and are indicative of ECM remodeling hallmarked by increased collagen synthesis, elastin degradation/fragmentation, and tissue stiffening (71–79). GO results from the transcriptomic analysis also showed enrichment of genes involved in ECM modification, including *Mmp3* and *Col13a1*, further supporting the SCI-induced ECM remodeling hypothesis. Vascular ECM stiffening/remodeling resulting from SCI likely impacts the myogenic response more than the TGF mechanism of renal autoregulation. Reasonably, increased stiffening could potentially alter the expression or sensitivity of mechanosensors that are repeatedly activated and deactivated due to continuous variations in RPP, particularly during AD causing acute fluctuations in systemic pressure. Such changes in mechanosensors could impair smooth muscle contractile signaling activation, and thus myogenic response and autoregulation of blood flow to the kidney, as seen in T3Tx SCI mice. Furthermore, increased ECM stiffening could reduce vascular compliance, thereby increasing rigidity and reducing the capacity of smooth muscle cells to stretch for the activation of mechanotransduction in response to increases in intraluminal pressure. It would be interesting to investigate these potential causal relationships between ECM remodeling and impairment of myogenic response as a mechanistic basis for renal autoregulation failure that hallmarks high thoracic-level SCI.

Results from the transcriptomic analysis of bulk kidney RNA also suggest the immune and inflammatory responses are the mechanisms by which thoracic SCI leads to kidney injury and dysfunction. For instance, pathway analysis showed perturbation of genes in the cytokine-cytokine receptor signaling pathway after both T3 and T10 SCI, whereas perturbation of genes in the chemokine signaling pathway was observed only after T3 SCI. This difference was underscored by increased expression of *Cxcl10* in kidneys weeks after only T3Tx. The elevation of circulating levels of inflammatory markers including IL-6 in the acute phase and SAA1 in the acute and chronic phase of both injury types further support the involvement of tissue inflammation in SCI-induced kidney injury. Inflammation and the immune response are well established to play key roles in tissue injury, including neuronal loss, vascular leakage, and scar formation at or near the site of SCI (80–87) and in ischemic-reperfusion injury of the kidney (88, 89). Whether global inflammation and/or the immune response mediate injury of organs distant from the site of SCI, including the kidney, should be explored and directly tested in future studies.

Despite the robust structural and functional differences of the effects of SCI on renal hemodynamics, there are a few caveats of the experimental approach that limit the interpretation of the results and warrant additional studies for detailed mechanistic understanding of kidney dysfunction resulting from thoracic SCI. For instance, basal renal hemodynamics and response to vasoactive agents

were assessed under isoflurane anesthesia, which is known to affect autonomic function and levels of vasoactive hormones in the circulation (90–92), the very factors that are directly and markedly impacted by SCI. Thus, a more rigorous assessment of renal dysfunction after SCI should include the measurement of GFR and RBF under conscious and unrestrained conditions. As the results show, SCI-induced renal dysfunction is associated with ECM remodeling and activation of local cytokine/chemokine signaling. However, the causal link between these changes and renal hemodynamics remains to be elucidated, and such future studies should use animal models that permit the tuning of vascular ECM stiffness and/or pharmacological targeting of candidate signaling pathways involved in vascular tone regulation and thus renal autoregulation.

In conclusion, our results show that the level of SCI is a key determinant to the severity and progression of kidney damage and dysfunction. This study provides the first evidence for the potential involvement of ECM remodeling and inflammatory cytokine/chemokine signaling in the pathogenesis of renal injury and hemodynamics impairment resulting from SCI. Further studies that elucidate the underlying molecular mechanisms will be crucial to identifying novel therapeutic targets for treating renal dysfunction and associated urinary complications, including excessive urine production and bladder distension, and autonomic failure in chronic SCI.

SUPPLEMENTAL DATA

Supplemental Tables S1—S4: https://doi.org/10.6084/m9.figshare.19379978.v1.

ACKNOWLEDGMENTS

We thank Dr. Alexander G. Rabchevsky for providing the MATLAB algorithm for the analysis of naturally occurring autonomic dysreflexia events and the Drexel University Spinal Cord Research Center for use of its core facilities. We thank all members of the Osei-Owusu and Tom laboratories for technical support.

GRANTS

This work was supported by Craig H. Neilsen Foundation Grant 382566 (to V.J.T. and P.O.-O), National Institutes of Health Grants R01NS1069080, R01NS111761, R01NS085426, and R01NS122371 (to V.J.T.) and R01HL139754 (to P.O.-O.), and American Heart Association Scientist Development Grant 16SDG27260276 (to P.O.-O.).

DISCLOSURES

No conflicts of interest, financial or otherwise, are declared by the authors.

AUTHOR CONTRIBUTIONS

P.O.-O. and V.J.T. conceived and designed research; P.O.-O., E.C., and S.A.D. performed experiments; P.O.-O., E.C., S.A.D., R.E.A., and V.J.T. analyzed data; P.O.-O. and V.J.T. interpreted results of experiments; P.O.-O., E.C., R.E.A., and V.J.T. prepared figures; P.O.-O. and V.J.T. drafted manuscript; P.O.-O., E.C., S.A.D., R.E.A., and V.J.T. edited and revised manuscript; P.O.-O. and V.J.T. approved final version of manuscript.

REFERENCES

1. **Savic G**, **DeVivo MJ**, **Frankel HL**, **Jamous MA**, **Soni BM**, **Charlifue S.** Causes of death after traumatic spinal cord injury-a 70-year British study. *Spinal Cord* 55: 891–897, 2017. doi:10.1038/sc.2017.64.
2. **Partida E**, **Mironets E**, **Hou S**, **Tom VJ.** Cardiovascular dysfunction following spinal cord injury. *Neural Regen Res* 11: 189–194, 2016. doi:10.4103/1673-5374.177707.
3. **Viaene A**, **Denys M-A**, **Goessaert A-S**, **Claeys J**, **Raes A**, **Roggeman S**, **Everaert K.** Evaluation of the occurrence and diagnose definitions for nocturnal polyuria in spinal cord injured patients during rehabilitation. *Eur J Phys Rehabil Med* 55: 40–46, 2019. doi:10.23736/S1973-9087.17.04851-1.
4. **Kuhlemeier KV**, **McEachran AB**, **Lloyd LK**, **Stover SL**, **Tauxe WN**, **Dubovsky EV**, **Fine PR.** Renal function after acute and chronic spinal cord injury. *J Urol* 131: 439–445, 1984. doi:10.1016/s0022-5347(17)50441-3.
5. **Szollar SM**, **Dunn KL**, **Brandt S**, **Fincher J.** Nocturnal polyuria and antidiuretic hormone levels in spinal cord injury. *Arch Phys Med Rehabil* 78: 455–458, 1997. doi:10.1016/s0003-9993(97)90155-6.
6. **Montgomery LR**, **Hubscher CH.** Altered vasopressin and natriuretic peptide levels in a rat model of spinal cord injury: implications for the development of polyuria. *Am J Physiol Renal Physiol* 314: F58–F66, 2018. doi:10.1152/ajprenal.00229.2017.
7. **Denys M-A**, **Viaene A**, **Goessaert A-S**, **Van Haverbeke F**, **Hoebeke P**, **Raes A**, **Everaert K.** Circadian rhythms in water and solute handling in adults with a spinal cord injury. *J Urol* 197: 445–451, 2017. doi:10.1016/j.juro.2016.08.001.
8. **Kilinc S**, **Akman MN**, **Levendoglu F**, **Ozker R.** Diurnal variation of antidiuretic hormone and urinary output in spinal cord injury. *Spinal Cord* 37: 332–335, 1999. doi:10.1038/sj.sc.3100814.
9. **Inoue T**, **Nonoguchi H**, **Tomita K.** Physiological effects of vasopressin and atrial natriuretic peptide in the collecting duct. *Cardiovasc Res* 51: 470–480, 2001. doi:10.1016/s0008-6363(01)00248-6.
10. **Lee HW**, **Choo M-S**, **Lee JG**, **Park CH**, **Paick J-S**, **Lee JZ**, **Han DH**, **Park WH**, **Lee K-S.** Desmopressin is an effective treatment for mixed nocturia with nocturnal polyuria and decreased nocturnal bladder capacity. *J Korean Med Sci* 25: 1792–1797, 2010. doi:10.3346/jkms.2010.25.12.1792.
11. **Zahariou A**, **Karagiannis G**, **Papaioannou P**, **Stathi K**, **Michail X.** The use of desmopressin in the management of nocturnal enuresis in patients with spinal cord injury. *Eura Medicophys* 43: 333–338, 2007.
12. **Rodríguez-Romero V**, **Guízar-Sahagún G**, **Castañeda-Hernández G**, **Reyes JL**, **Cruz-Antonio L.** Early systemic alterations in severe spinal cord injury: an experimental study on the impact of injury level on renal function. *Spine* 43: E885–E890, 2018. doi:10.1097/BRS.0000000000002578.
13. **Karlsson AK.** Autonomic dysfunction in spinal cord injury: clinical presentation of symptoms and signs. *Prog Brain Res* 152: 1–8, 2006. doi:10.1016/S0079-6123(05)52034-X.
14. **Gumz ML.** Molecular basis of circadian rhythmicity in renal physiology and pathophysiology. *Exp Physiol* 101: 1025–1029, 2016. doi:10.1113/EP085781.
15. **Crowley SD**, **Coffman TM.** In hypertension, the kidney breaks your heart. *Curr Cardiol Rep* 10: 470–476, 2008. doi:10.1007/s11886-008-0074-5.
16. **Orlov SN**, **Mongin AA.** Salt-sensing mechanisms in blood pressure regulation and hypertension. *Am J Physiol Heart Circ Physiol* 293: H2039–H2053, 2007. doi:10.1152/ajpheart.00325.2007.
17. **Hall JE**, **Granger JP**, **do Carmo JM**, **da Silva AA**, **Dubinion J**, **George E**, **Hamza S**, **Speed J**, **Hall ME.** Hypertension: physiology and pathophysiology. *Compr Physiol* 2: 2393–2442, 2012. doi:10.1002/cphy.c110058.
18. **Fleming SJ**, **Dallemagne CR**, **Endre ZH**, **Yesberg NE**, **Cross RB.** Acute lowering of plasma oncotic pressure increases filtration fraction and sodium excretion in conscious sheep. *Ren Physiol Biochem* 15: 334–340, 1992. doi:10.1159/000173470.

19. **Knox FG**, **Cuche JL**, **Ott CE**, **Diaz-Buxo JA**, **Marchand G.** Regulation of glomerular filtration and proximal tubule reabsorption. *Circ Res* 36: 107–118, 1975. doi:10.1161/01.res.36.6.107.
20. **Guyton AC.** Blood pressure control–special role of the kidneys and body fluids. *Science* 252: 1813–1816, 1991. doi:10.1126/science.2063193.
21. **Guyton AC.** Dominant role of the kidneys and accessory role of whole-body autoregulation in the pathogenesis of hypertension. *Am J Hypertens* 2: 575–585, 1989. doi:10.1093/ajh/2.7.575.
22. **Aukland K.** Myogenic mechanisms in the kidney. *J Hypertens Suppl* 7: S71–S76, 1989.
23. **Carlström M**, **Wilcox CS**, **Arendshorst WJ.** Renal autoregulation in health and disease. *Physiol Rev* 95: 405–511, 2015. doi:10.1152/physrev.00042.2012.
24. **A Mitrou NG**, **Cupples WA.** Renal blood flow dynamics in inbred rat strains provides insight into autoregulation. *Curr Vasc Pharmacol* 12: 801–809, 2014. doi:10.2174/15701611113116660154.
25. **Burke M**, **Pabbidi MR**, **Farley J**, **Roman RJ.** Molecular mechanisms of renal blood flow autoregulation. *Curr Vasc Pharmacol* 12: 845–858, 2014. doi:10.2174/1570161113116660149.
26. **Li L**, **Lai EY**, **Huang Y**, **Eisner C**, **Mizel D**, **Wilcox CS**, **Schnermann J.** Renal afferent arteriolar and tubuloglomerular feedback reactivity in mice with conditional deletions of adenosine 1 receptors. *Am J Physiol Renal Physiol* 303: F1166–F1175, 2012. doi:10.1152/ajprenal.00222.2012.
27. **Grifoni SC**, **Chiposi R**, **McKey SE**, **Ryan MJ**, **Drummond HA.** Altered whole kidney blood flow autoregulation in a mouse model of reduced β-ENaC. *Am J Physiol Renal Physiol* 298: F285–F292, 2010. doi:10.1152/ajprenal.00496.2009.
28. **Loutzenhiser R**, **Griffin K**, **Williamson G**, **Bidani A.** Renal autoregulation: new perspectives regarding the protective and regulatory roles of the underlying mechanisms. *Am J Physiol Regul Integr Comp Physiol* 290: R1153–R1167, 2006. doi:10.1152/ajpregu.00402.2005.
29. **Just A**, **Arendshorst WJ.** Dynamics and contribution of mechanisms mediating renal blood flow autoregulation. *Am J Physiol Regul Integr Comp Physiol* 285: R619–R631, 2003. doi:10.1152/ajpregu.00766.2002.
30. **Cupples WA**, **Braam B.** Assessment of renal autoregulation. *Am J Physiol Renal Physiol* 292: F1105–F1123, 2007. doi:10.1152/ajprenal.00194.2006.
31. **Mironets E**, **Osei-Owusu P**, **Bracchi-Ricard V**, **Fischer R**, **Owens EA**, **Ricard J**, **Wu D**, **Saltos T**, **Collyer E**, **Hou S**, **Bethea JR**, **Tom VJ.** Soluble TNFα signaling within the spinal cord contributes to the development of autonomic dysreflexia and ensuing vascular and immune dysfunction after spinal cord injury. *J Neurosci* 38: 4146–4162, 2018. doi:10.1523/JNEUROSCI.2376-17.2018.
32. **Hou S**, **Saltos TM**, **Iredia IW**, **Tom VJ.** Surgical techniques influence local environment of injured spinal cord and cause various grafted cell survival and integration. *J Neurosci Methods* 293: 144–150, 2018. doi:10.1016/j.jneumeth.2017.09.014.
33. **O'Reilly ML**, **Mironets E**, **Shapiro TM**, **Crowther K**, **Collyer E**, **Bethea JR**, **Tom VJ.** Pharmacological inhibition of soluble tumor necrosis factor-alpha two weeks after high thoracic spinal cord injury does not affect sympathetic hyperreflexia. *J Neurotrauma* 38: 2186–2191, 2021. doi:10.1089/neu.2020.7504.
34. **Osei-Owusu P**, **Owens EA**, **Jie L**, **Reis JS**, **Forrester SJ**, **Kawai T**, **Eguchi S**, **Singh H**, **Blumer KJ.** Regulation of renal hemodynamics and function by RGS2. *PLoS One* 10: e0132594, 2015. doi:10.1371/journal.pone.0132594.
35. **Meleka MM.** Anti-hypertensive mechanisms of cyclic depsipeptide inhibitor ligands for $G_{q/11}$ class G proteins. *Pharmacol Res* 141: 264–275, 2019. doi:10.1016/j.phrs.2019.01.012.
36. **Owens EA**, **Jie L**, **Reyes BAS**, **Van Bockstaele EJ**, **Osei-Owusu P.** Elastin insufficiency causes hypertension, structural defects and abnormal remodeling of renal vascular signaling. *Kidney Int* 92: 1100–1118, 2017. doi:10.1016/j.kint.2017.04.044.
37. **Mironets E**, **Fischer R**, **Bracchi-Ricard V**, **Saltos TM**, **Truglio TS**, **O'Reilly ML**, **Swanson KA**, **Bethea JR**, **Tom VJ.** Attenuating neurogenic sympathetic hyperreflexia robustly improves antibacterial immunity after chronic spinal cord injury. *J Neurosci* 40: 478–492, 2020. doi:10.1523/JNEUROSCI.2417-19.2019.
38. **Mayorov DN**, **Adams MA**, **Krassioukov AV.** Telemetric blood pressure monitoring in conscious rats before and after compression injury of spinal cord. *J Neurotrauma* 18: 727–736, 2001. doi:10.1089/089771501750357663.
39. **Mathias CJ.** Orthostatic hypotension and paroxysmal hypertension in humans with high spinal cord injury. *Prog Brain Res* 152: 231–243, 2006. doi:10.1016/S0079-6123(05)52015-6.
40. **Laird AS**, **Carrive P**, **Waite PM.** Cardiovascular and temperature changes in spinal cord injured rats at rest and during autonomic dysreflexia. *J Physiol* 577: 539–548, 2006. doi:10.1113/jphysiol.2006.116301.
41. **Hayes KC**, **Hull TCL**, **Delaney GA**, **Potter PJ**, **Sequeira KAJ**, **Campbell K**, **Popovich PG.** Elevated serum titers of proinflammatory cytokines and CNS autoantibodies in patients with chronic spinal cord injury. *J Neurotrauma* 19: 753–761, 2002. doi:10.1089/08977150260139129.
42. **Zhang Y**, **Guan Z**, **Reader B**, **Shawler T**, **Mandrekar-Colucci S**, **Huang K**, **Weil Z**, **Bratasz A**, **Wells J**, **Powell ND**, **Sheridan JF**, **Whitacre CC**, **Rabchevsky AG**, **Nash MS**, **Popovich PG.** Autonomic dysreflexia causes chronic immune suppression after spinal cord injury. *J Neurosci* 33: 12970–12981, 2013. doi:10.1523/JNEUROSCI.1974-13.2013.
43. **Brennan FH**, **Noble BT**, **Wang Y**, **Guan Z**, **Davis H**, **Mo X**, **Harris C**, **Eroglu C**, **Ferguson AR**, **Popovich PG.** Acute post-injury blockade of α2δ-1 calcium channel subunits prevents pathological autonomic plasticity after spinal cord injury. *Cell Rep* 34: 108667, 2021. doi:10.1016/j.celrep.2020.108667.
44. **Krassioukov AV**, **Weaver LC.** Episodic hypertension due to autonomic dysreflexia in acute and chronic spinal cord-injured rats. *Am J Physiol Heart Circ Physiol* 268: H2077–H2083, 1995. doi:10.1152/ajpheart.1995.268.5.H2077.
45. **Curt A**, **Nitsche B**, **Rodic B**, **Schurch B**, **Dietz V.** Assessment of autonomic dysreflexia in patients with spinal cord injury. *J Neurol Neurosurg Psychiatry* 62: 473–477, 1997. doi:10.1136/jnnp.62.5.473.
46. **Munakata M**, **Kameyama J**, **Kanazawa M**, **Nunokawa T**, **Moriai N**, **Yoshinaga K.** Circadian blood pressure rhythm in patients with higher and lower spinal cord injury: simultaneous evaluation of autonomic nervous activity and physical activity. *J Hypertens* 15: 1745–1749, 1997. doi:10.1097/00004872-199715120-00083.
47. **Anthony DC**, **Couch Y.** The systemic response to CNS injury. *Exp Neurol* 258: 105–111, 2014. doi:10.1016/j.expneurol.2014.03.013.
48. **Goh MY**, **Millard MS**, **Wong ECK**, **Brown DJ**, **Frauman AG**, **O'Callaghan CJ.** Diurnal blood pressure and urine production in acute spinal cord injury compared with controls. *Spinal Cord* 55: 39–46, 2017. doi:10.1038/sc.2016.100.
49. **Dustan HP.** Physiologic regulation of arterial pressure: an overview. *Hypertension* 4: III62–III67, 1982. doi:10.1161/01.hyp.4.5_pt_2.iii62.
50. **Sutters M**, **Wakefield C**, **O'Neil K**, **Appleyard M**, **Frankel H**, **Mathias CJ**, **Peart WS.** The cardiovascular, endocrine and renal response of tetraplegic and paraplegic subjects to dietary sodium restriction. *J Physiol* 457: 515–523, 1992. doi:10.1113/jphysiol.1992.sp019391.
51. **Gibbons GH**, **Dzau VJ**, **Farhi ER**, **Barger AC.** Interaction of signals influencing renin release. *Annu Rev Physiol* 46: 291–308, 1984. doi:10.1146/annurev.ph.46.030184.001451.
52. **Nitsche B**, **Perschak H**, **Curt A**, **Dietz V.** Loss of circadian blood pressure variability in complete tetraplegia. *J Hum Hypertens* 10: 311–317, 1996.
53. **Landry E**, **Frenette J**, **Guertin PA.** Body weight, limb size, and muscular properties of early paraplegic mice. *J Neurotrauma* 21: 1008–1016, 2004. doi:10.1089/0897715041651060.
54. **Fang Y**, **Morse LR**, **Nguyen N**, **Tsantes NG**, **Troy KL.** Anthropometric and biomechanical characteristics of body segments in persons with spinal cord injury. *J Biomech* 55: 11–17, 2017. doi:10.1016/j.jbiomech.2017.01.036.
55. **Scholpa NE**, **Simmons EC**, **Tilley DG**, **Schnellmann RG.** β2-adrenergic receptor-mediated mitochondrial biogenesis improves skeletal muscle recovery following spinal cord injury. *Exp Neurol* 322: 113064, 2019. doi:10.1016/j.expneurol.2019.113064.
56. **Hayes BD**, **Fossey MPM**, **Poormasjedi-Meibod MS**, **Erskine E**, **Soriano JE**, **Scott B**, **Rosentreter R**, **Granville DJ**, **Phillips AA**, **West CR.** Experimental high thoracic spinal cord injury impairs the cardiac and cerebrovascular response to orthostatic challenge in rats. *Am J Physiol Heart Circ Physiol* 321: H716–H727, 2021. doi:10.1152/ajpheart.00239.2021.
57. **West CR**, **Popok D**, **Crawford MA**, **Krassioukov AV.** Characterizing the temporal development of cardiovascular dysfunction in response to spinal cord injury. *J Neurotrauma* 32: 922–930, 2015. doi:10.1089/neu.2014.3722.

58. **Hall JE.** The renin-angiotensin system: renal actions and blood pressure regulation. *Compr Ther* 17: 8–17, 1991.
59. **Takenaka T**, **Suzuki H**, **Fujiwara K**, **Kanno Y**, **Ohno Y**, **Hayashi K**, **Nagahama T**, **Saruta T.** Cellular mechanisms mediating rat renal microvascular constriction by angiotensin II. *J Clin Investig* 100: 2107–2114, 1997. doi:10.1172/JCI119745.
60. **Arendshorst WJ**, **Brannstrom K**, **Ruan X.** Actions of angiotensin II on the renal microvasculature. *J Am Soc Nephrol* 10, *Suppl* 11: S149–S161, 1999.
61. **Arima S.** Role of angiotensin II and endogenous vasodilators in the control of glomerular hemodynamics. *Clin Exp Nephrol* 7: 172–178, 2003. doi:10.1007/s10157-003-0249-8.
62. **Feng MG**, **Navar LG.** Angiotensin II-mediated constriction of afferent and efferent arterioles involves T-type Ca^{2+} channel activation. *Am J Nephrol* 24: 641–648, 2004. doi:10.1159/000082946.
63. **Brinks HL**, **Eckhart AD.** Regulation of GPCR signaling in hypertension. *Biochim Biophys Acta* 1802: 1268–1275, 2010. doi:10.1016/j.bbadis.2010.01.005.
64. **Kim HJ**, **Jang JH**, **Zhang YH**, **Yoo HY**, **Kim SJ.** Fast relaxation and desensitization of angiotensin II contraction in the pulmonary artery via AT1R and Akt-mediated phosphorylation of muscular eNOS. *Pflugers Arch* 471: 1317–1330, 2019. doi:10.1007/s00424-019-02305-z.
65. **Simoes e Silva AC**, **Silveira KD**, **Ferreira AJ**, **Teixeira MM.** ACE2, angiotensin-(1-7) and Mas receptor axis in inflammation and fibrosis. *Br J Pharmacol* 169: 477–492, 2013. doi:10.1111/bph.12159.
66. **Potthoff SA**, **Fähling M**, **Clasen T**, **Mende S**, **Ishak B**, **Suvorava T**, **Stamer S**, **Thieme M**, **Sivritas SH**, **Kojda G**, **Patzak A**, **Rump LC**, **Stegbauer J.** Angiotensin-(1-7) modulates renal vascular resistance through inhibition of p38 mitogen-activated protein kinase in apolipoprotein E-deficient mice. *Hypertension* 63: 265–272, 2014. doi:10.1161/HYPERTENSIONAHA.113.02289.
67. **Kuczeriszka M**, **Kompanowska-Jezierska E**, **Sadowski J**, **Prieto MC**, **Navar LG.** Modulating role of Ang1-7 in control of blood pressure and renal function in AngII-infused hypertensive rats. *Am J Hypertens* 31: 504–511, 2018. doi:10.1093/ajh/hpy006.
68. **Kanda T**, **Itoh H.** The ACE2/Ang(1-7)/Mas receptor axis in cardiovascular and renal diseases. *Nihon Rinsho* 70: 1487–1491, 2012.
69. **Trueblood CT**, **Iredia IW**, **Collyer ES**, **Tom VJ**, **Hou S.** Development of cardiovascular dysfunction in a rat spinal cord crush model and responses to serotonergic interventions. *J Neurotrauma* 36: 1478–1486, 2019. doi:10.1089/neu.2018.5962.
70. **Hou S**, **Lu P**, **Blesch A.** Characterization of supraspinal vasomotor pathways and autonomic dysreflexia after spinal cord injury in F344 rats. *Auton Neurosci* 176: 54–63, 2013. doi:10.1016/j.autneu.2013.02.001.
71. **Lacolley P**, **Boutouyrie P**, **Glukhova M**, **Daniel Lamaziere J-M**, **Plouin P-F**, **Bruneval P**, **Vuong P**, **Corvol P**, **Laurent S.** Disruption of the elastin gene in adult Williams syndrome is accompanied by a paradoxical reduction in arterial stiffness. *Clin Sci (Lond)* 103: 21–29, 2002. doi:10.1042/CS20010287.
72. **Karnik SK**, **Brooke BS**, **Bayes-Genis A**, **Sorensen L**, **Wythe JD**, **Schwartz RS**, **Keating MT**, **Li DY.** A critical role for elastin signaling in vascular morphogenesis and disease. *Development* 130: 411–423, 2003. doi:10.1242/dev.00223.
73. **Kelleher CM**, **McLean SE**, **Mecham RP.** Vascular extracellular matrix and aortic development. *Curr Top Dev Biol* 62: 153–188, 2004. doi:10.1016/S0070-2153(04)62006-0.
74. **Pai AS**, **Giachelli CM.** Matrix remodeling in vascular calcification associated with chronic kidney disease. *J Am Soc Nephrol* 21: 1637–1640, 2010. doi:10.1681/ASN.2010040349.
75. **Rüster C**, **Wolf G.** Angiotensin II as a morphogenic cytokine stimulating renal fibrogenesis. *J Am Soc Nephrol* 22: 1189–1199, 2011. doi:10.1681/ASN.2010040384.
76. **Martínez-Revelles S**, **García-Redondo AB**, **Avendaño MS**, **Varona S**, **Palao T**, **Orriols M**, **Roque FR**, **Fortuño A**, **Touyz RM**, **Martínez-González J**, **Salaices M**, **Rodríguez C**, **Briones AM.** Lysyl oxidase induces vascular oxidative stress and contributes to arterial stiffness and abnormal elastin structure in hypertension: role of p38MAPK. *Antioxid Redox Signal* 27: 379–397, 2017. doi:10.1089/ars.2016.6642.
77. **Jacob MP**, **Badier-Commander C**, **Fontaine V**, **Benazzoug Y**, **Feldman L**, **Michel JB.** Extracellular matrix remodeling in the vascular wall. *Pathol Biol (Paris)* 49: 326–332, 2001. doi:10.1016/s0369-8114(01)00151-1.
78. **Briones AM**, **Arribas SM**, **Salaices M.** Role of extracellular matrix in vascular remodeling of hypertension. *Curr Opin Nephrol Hypertens* 19: 187–194, 2010. doi:10.1097/MNH.0b013e328335eec9.
79. **Halper J.** Basic components of vascular connective tissue and extracellular matrix. *Adv Pharmacol* 81: 95–127, 2018. doi:10.1016/bs.apha.2017.08.012.
80. **Lee JY**, **Choi HY**, **Ahn HJ**, **Ju BG**, **Yune TY.** Matrix metalloproteinase-3 promotes early blood-spinal cord barrier disruption and hemorrhage and impairs long-term neurological recovery after spinal cord injury. *Am J Pathol* 184: 2985–3000, 2014. doi:10.1016/j.ajpath.2014.07.016.
81. **Papakostas JC**, **Matsagas MI**, **Toumpoulis IK**, **Malamou-Mitsi VD**, **Pappa LS**, **Gkrepi C**, **Anagnostopoulos CE**, **Kappas AM.** Evolution of spinal cord injury in a porcine model of prolonged aortic occlusion. *J Surg Res* 133: 159–166, 2006. doi:10.1016/j.jss.2005.10.007.
82. **Bethea JR**, **Nagashima H**, **Acosta MC**, **Briceno C**, **Gomez F**, **Marcillo AE**, **Loor K**, **Green J**, **Dietrich WD.** Systemically administered interleukin-10 reduces tumor necrosis factor-alpha production and significantly improves functional recovery following traumatic spinal cord injury in rats. *J Neurotrauma* 16: 851–863, 1999. doi:10.1089/neu.1999.16.851.
83. **Pan JZ**, **Ni L**, **Sodhi A**, **Aguanno A**, **Young W**, **Hart RP.** Cytokine activity contributes to induction of inflammatory cytokine mRNAs in spinal cord following contusion. *J Neurosci Res* 68: 315–322, 2002. doi:10.1002/jnr.10215.
84. **Weaver LC**, **Marsh DR**, **Gris D**, **Brown A**, **Dekaban GA.** Autonomic dysreflexia after spinal cord injury: central mechanisms and strategies for prevention. *Prog Brain Res* 152: 245–263, 2006. doi:10.1016/S0079-6123(05)52016-8.
85. **Brewer KL**, **Bethea JR**, **Yezierski RP.** Neuroprotective effects of interleukin-10 following excitotoxic spinal cord injury. *Exp Neurol* 159: 484–493, 1999. doi:10.1006/exnr.1999.7173.
86. **Beattie MS.** Inflammation and apoptosis: linked therapeutic targets in spinal cord injury. *Trends Mol Med* 10: 580–583, 2004. doi:10.1016/j.molmed.2004.10.006.
87. **Chan CC.** Inflammation: beneficial or detrimental after spinal cord injury? *Recent Pat CNS Drug Discov* 3: 189–199, 2008. doi:10.2174/157488908786242434.
88. **Bonventre JV.** Pathophysiology of acute kidney injury: roles of potential inhibitors of inflammation. *Contrib Nephrol* 156: 39–46, 2007. doi:10.1159/000102069.
89. **Brøchner AC**, **Dagnaes-Hansen F**, **Højberg-Holm J**, **Toft P.** The inflammatory response in blood and in remote organs following acute kidney injury. *APMIS* 122: 399–404, 2014. doi:10.1111/apm.12157.
90. **Ullman J**, **Härgestam R**, **Lindahl S**, **Chan SHH**, **Eriksson S**, **Rundgren M.** Circulatory effects of angiotensin II during anaesthesia, evaluated by real-time spectral analysis. *Acta Anaesthesiol Scand* 47: 532–540, 2003. doi:10.1034/j.1399-6576.2003.00114.x.
91. **Nakamura T**, **Ogawa S**, **Saeki S**, **Kato J.** Suppressive effect of isoflurane on somato-sympathetic reflexes in cats. *Masui* 47: 678–689, 1998.
92. **Kiriyama M**, **Haji A**, **Masuda A**, **Ito Y**, **Takeda R.** Effects of isoflurane on brain stem blood flow and renal sympathetic nerve activity during induced hypotension. *Pharmacology* 54: 232–240, 1997. doi:10.1159/000139491.